

Fermi surface segmentation in the helical state of a Rashba superconductor

Alireza Akbari ^{1,2} and Peter Thalmeier¹

¹Max Planck Institute for the Chemical Physics of Solids, D-01187 Dresden, Germany

²Max Planck POSTECH Center for Complex Phase Materials, and Department of Physics, POSTECH, Pohang, Gyeongbuk 790-784, Korea



(Received 24 January 2022; revised 22 March 2022; accepted 12 April 2022; published 3 May 2022)

We investigate the quasiparticle excitations in the Fulde-Ferrell-type helical state of a superconductor with inversion symmetry breaking and strong Rashba spin-orbit coupling. We restrict to a state with single finite momentum of Cooper pairs in the helical phase that is determined by minimization of the condensation energy. We derive the dependence of quasiparticle dispersions on the Rashba coupling strength and external field. It leads to a peculiar momentum-space segmentation of the corresponding Rashba Fermi surface sheets. We show that it may be directly visualized by the method of quasiparticle interference that identifies the critical points of the segmented sheets and can map their evolution with field strength, bias voltage, and Rashba coupling. We also indicate a strategy for how to determine the finite Cooper-pair momentum from experimental quantities. This investigation has the potential for a more detailed microscopic understanding of the helical superconducting state under the influence of Rashba spin-orbit coupling.

DOI: [10.1103/PhysRevResearch.4.023096](https://doi.org/10.1103/PhysRevResearch.4.023096)

I. INTRODUCTION

In a superconductor (SC) with small orbital pair breaking a new state may become stable at larger fields where the conduction electrons are not bound in BCS pairs ($-\mathbf{k} \uparrow$, $\mathbf{k} \downarrow$) but rather in pairs ($-\mathbf{k} + \mathbf{q} \uparrow$, $\mathbf{k} + \mathbf{q} \downarrow$) with finite center-of-mass momentum $2\mathbf{q}$ characterized by a gap function $\Delta(\mathbf{r}) = \Delta_{\mathbf{q}} \exp(i\mathbf{q}\mathbf{r})$. This Fulde-Ferrell (FF) state [1] and the related Larkin-Ovchinnikov (LO) state [2] with both (\mathbf{q} , $-\mathbf{q}$) momenta involved is well studied theoretically, in superconductors of various dimensionality [3,4] as well as in condensed quantum gases [5,6]. Convincing evidence for the experimental realization of this state at low temperatures and high fields is, however, rather scarce, which may be due to the sensitivity to impurities [7–9] and orbital pair breaking [10,11]. There are unconventional heavy fermion superconductors [8] and organic superconductors [12,13] as well as Fe pnictides [14,15] where its appearance has been suggested. The existence of the FF or LO phases in these cases is mostly inferred from thermodynamic anomalies [16] in the low-temperature high-field sector of the phase diagram or from NMR experiments [17] and they may be used to map out the phase boundaries.

However, such experiments do not address the microscopic nature of this state deep inside the FF-type phase. The latter, to which we will exclusively restrict, is stabilized by a tradeoff between the loss of condensation energy due to the kinetic

energy of pairs with center of mass momentum and gain in Zeeman energy due to population imbalance of spin states [18,19]. This tradeoff depends on the momentum position on the Fermi surface (FS) and therefore generally the latter is segmented into regions where the pairs are still stable with finite $2\mathbf{q}$ (paired region) and where they are unstable (unpaired region). The relative size of these FS segments depends on the field strength with the paired region vanishing above the critical field of the FF phase. This microscopic structure of the FF state has not been probed in practice due to lack of suitable techniques. It was proposed in Ref. [20] that the scanning tunneling microscopy (STM) based quasiparticle interference (QPI) method is a promising candidate for this purpose. However, as a feasibility study only the inversion symmetric superconductor was investigated in this paper.

In reality inversion symmetry at the superconductor surface is broken and some of the promising SC materials have layered structure with broken two-dimensional (2D) inversion symmetry in the layers or even have bulk noncentrosymmetric structure with complete lack of inversion symmetry. Then Rashba-type spin-orbit coupling exists and will greatly modify both the FF-type states as well as QPI spectral features. In particular the Fermi surface will be doubled into two Rashba Fermi surfaces with different spin texture. This important case is therefore worthy of a separate theoretical investigation presented in this paper. There is an important distinction, however, to the common FF case where the Zeeman term leads to different Fermi sphere radii of up and down spin electrons, whereas under the presence of a dominating Rashba coupling the two Rashba band ($\lambda = \pm 1$) Fermi spheres are shifted perpendicular to the field by a certain amount proportional to the field strength. This leads immediately to stable Cooper pairs with finite momentum $2\mathbf{q}$ that grows with field strength characterized by a (s -wave) gap function $\Delta_{\mathbf{q}\lambda} \exp(i\mathbf{q}\mathbf{r})$. This commonly called “helical” state [21] is therefore of the FF

Published by the American Physical Society under the terms of the [Creative Commons Attribution 4.0 International license](https://creativecommons.org/licenses/by/4.0/). Further distribution of this work must maintain attribution to the author(s) and the published article's title, journal citation, and DOI. Open access publication funded by the Max Planck Society.

type but has a somewhat different composition of the condensation energy than in the original Zeeman dominated FF case.

Some aspects of the helical state including Rashba coupling and Zeeman term have been studied before, concerning mostly critical field curves [22–25]. Here we focus on the microscopic consequences of the Rashba coupling and its image in the QPI spectrum [26]. As a prerequisite we derive the quasiparticle excitation spectrum in the paired and unpaired segments of momentum space the sizes of which depend on the field strength. The corresponding QPI spectrum is created by scattering of quasiparticles from randomly distributed dilute impurities at the surface. We consider normal charge as well as Ising-type magnetic impurities. Our momentum-resolved QPI analysis has a twofold aim: Both the Rashba doubling of Fermi surface sheets as well as their segmentation in the helical state due to the appearance of unpaired states may be investigated as function of field strength, bias voltage, Rashba coupling, and chemical potential. In this way one may get a more microscopic understanding of the peculiar helical superconducting state. In particular we show that it is possible to obtain a direct experimental measure of the pair momentum $2\mathbf{q}$ by analyzing the characteristic wave vectors of the QPI image. The Rashba case with its helical phase is more amenable to such QPI analysis because the latter may appear already at small fields whereas the conventional FF phase requires generally very high fields.

The model for the Rashba superconductor is introduced in Sec. II and the Bogoliubov quasiparticle excitations are derived in Sec. III following a method introduced by Cui *et al.* in Ref. [27] for the inversion symmetric case without Rashba term (see also Ref. [20]). In Sec. IV we calculate the corresponding Green's functions and quasiparticle density of states (DOS) for the helical phase. In the main part of Sec. V we derive the QPI spectrum in Born approximation (BA) using a model for impurity scattering that contains both normal and magnetic scattering, transformed to the Rashba band states. Finally in Sec. VI we discuss the numerical results in detail and Sec. VII presents the summary and conclusion.

II. MODEL DEFINITION

Here we introduce the commonly used band-structure model including the Rashba coupling originating from inversion symmetry breaking. We use the periodic form to obtain the proper periodicity of spectral images in the later QPI calculations but we also relate this to the Rashba mechanism in parabolic approximation. The latter is more suitable for discussing fundamental properties of Rashba bands like the splitting of FS sheets and their shifting caused by the external field. Subsequently a minimal model for the superconducting state introduced in Ref. [21] will be briefly described and the Hamiltonian for the helical phase discussed.

A. Normal state Rashba bands and states

The 2D Rashba Hamiltonian in an external field is given by [21]

$$H_0 = \sum_{\mathbf{k}} \Psi_{\mathbf{k}}^\dagger h_{0\mathbf{k}} \Psi_{\mathbf{k}}, \quad h_{0\mathbf{k}} = \xi_{\mathbf{k}} \sigma_0 + (\alpha \mathbf{g}_{\mathbf{k}} + \mathbf{b}) \cdot \boldsymbol{\sigma}, \quad (1)$$

in the spin representation. Here $\Psi_{\mathbf{k}}^\dagger = (a_{\mathbf{k}\uparrow}^\dagger, a_{\mathbf{k}\downarrow}^\dagger)$ are conduction electron spinors and $\varepsilon_{\mathbf{k}} = -2t(\cos k_x + \cos k_y)$ with $-\pi \leq k_x, k_y \leq \pi$ is the periodic tight binding (TB) conduction band dispersion which is more suitable for the later treatment of the QPI spectrum. Here $t > 0$ is the hopping element leading to a conduction band half-width $D_c = 4t$ and $\xi_{\mathbf{k}} = \varepsilon_{\mathbf{k}} - \mu_{\text{TB}}$. The chemical potential μ_{TB} in the periodic band model therefore lies in the interval $-D_c \leq \mu_{\text{TB}} \leq D_c$ and is referenced to the *band center* $\varepsilon_{\mathbf{k}} = 0$. It is necessary to map this to the 2D parabolic band model for $\mu_{\text{TB}} \leq 0$ with $\varepsilon_{\mathbf{k}} = \varepsilon_0 + \mathbf{k}^2/2m$. Here $\varepsilon_0 = -D_c$ is the bottom of the band and $m = 2/D_c$ is its effective mass. The chemical potential referenced to the *band bottom* is then given by $\mu = \mu_{\text{TB}} - \varepsilon_0 \geq 0$. Furthermore $\mathbf{b} = \mu_B \mathbf{B}$ is the Zeeman energy scale given by the applied magnetic field \mathbf{B} . The inversion symmetry breaking Rashba spin-orbit coupling is odd under inversion with $\mathbf{g}_{-\mathbf{k}} = -\mathbf{g}_{\mathbf{k}}$, explicitly $\mathbf{g}_{\mathbf{k}}^p = (k_y, -k_x, 0)/k_F = (\sin \theta_{\mathbf{k}}, -\cos \theta_{\mathbf{k}}, 0)$ in the parabolic band model where $\theta_{\mathbf{k}}$ is the azimuthal angle of \mathbf{k} counted from the k_x axis where the Fermi wave number is $k_F = (2m\mu)^{1/2}$ and $v_F = k_F/m$ is the Fermi velocity. To stay consistent with the tight binding model dispersion we will take the periodic form

$$\mathbf{g}_{\mathbf{k}}^{\text{TB}} = (\sin k_y, -\sin k_x, 0), \quad (2)$$

where both forms are normalized, i.e., $|\mathbf{g}_{\mathbf{k}}^p| = 1$ and $|\mathbf{g}_{\mathbf{k}}^{\text{TB}}|_{\text{max}} = \sqrt{2}$. Equivalence in the limit of small wave vectors $k_x, k_y \ll \pi$ demands that the Rashba coupling constants in the two models are then related by $\alpha_P = k_F \alpha_{\text{TB}}$. We suppress indices TB and P in the following and rely on the context. Diagonalization of the Hamiltonian in Eq. (1) leads to

$$H_0 = \sum_{\mathbf{k}\lambda} \varepsilon_{\mathbf{k}\lambda} c_{\mathbf{k}\lambda}^\dagger c_{\mathbf{k}\lambda},$$

$$\varepsilon_{\mathbf{k}\lambda}(\mathbf{b}) = \xi_{\mathbf{k}} + \lambda |\alpha \mathbf{g}_{\mathbf{k}} + \mathbf{b}| \equiv \xi_{\mathbf{k}} + \lambda \zeta_{\mathbf{k}}^\pm, \quad (3)$$

where $\varepsilon_{\mathbf{k}\lambda}(\mathbf{b})$ denotes the Rashba split and Zeeman shifted bands (referred to μ) which have eigenfunctions corresponding to helicities $\lambda = \pm 1$. Here we introduce the auxiliary functions $\zeta_{\mathbf{k}}^\pm = |\alpha \mathbf{g}_{\mathbf{k}} \pm \mathbf{b}|$. In zero field the two Rashba bands are given by

$$\varepsilon_{\mathbf{k}\lambda}^0 = \xi_{\mathbf{k}} + \lambda |\alpha \mathbf{g}_{\mathbf{k}}| = \frac{1}{2m} (k + \lambda k_0)^2 - \tilde{\mu}, \quad (4)$$

where $k_0 = \frac{1}{2} \frac{|\alpha|}{\mu} k_F$ and $\tilde{\mu} = \mu (1 + \frac{1}{4} \frac{\alpha^2}{\mu^2})$. This describes two parabolic dispersions shifted by k_0 . The ensuing two Fermi spheres have radii given approximately by $k_F^\lambda = k_F - \lambda k_0 = k_F (1 - \frac{\lambda}{2} \frac{|\alpha|}{\mu})$ for moderate Rashba coupling $|\alpha| \ll \mu$. Then their relative difference $(k_F^- - k_F^+)/k_F = |\alpha|/\mu$ is a direct measure for the strength of the Rashba coupling. The operators $\Phi_{\mathbf{k}}^\dagger = (c_{\mathbf{k}+}^\dagger, c_{\mathbf{k}-}^\dagger)$ ($\lambda = \pm$) creating the helical eigenstates $|\mathbf{k}\lambda\rangle = c_{\mathbf{k}\lambda}^\dagger |0\rangle$ are obtained [28] from

$$\Phi_{\mathbf{k}}^\dagger = \Psi_{\mathbf{k}}^\dagger S_{\mathbf{k}}, \quad S_{\mathbf{k}} = \frac{1}{\sqrt{2}} \begin{bmatrix} 1 & ie^{-i\theta_{\mathbf{k}}} \\ ie^{i\theta_{\mathbf{k}}} & 1 \end{bmatrix}, \quad (5)$$

where $\theta_{\mathbf{k}} = -\tan^{-1}(g_{k_x}/g_{k_y}) = \tan^{-1}(\sin k_y/\sin k_x) \rightarrow \tan^{-1}(k_y/k_x)$ where the second and last expression correspond to TB and parabolic models, respectively. For finite but small in-plane field $\mathbf{b} = b(\cos \phi, \sin \phi, 0)$ ($b \ll \alpha$), where ϕ defines the

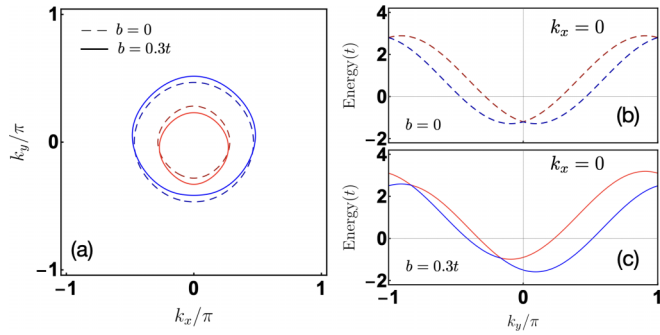


FIG. 1. (a) Splitting of Rashba Fermi surface sheets $\sim|\alpha|/\mu$ (dashed) and opposite shifting of their centers by $\pm q_s$ along the k_y axis for large field (full); blue/red, $\lambda = \pm 1$. Magnetic field $\mathbf{b} \parallel x$ axis and perpendicular shift vector $\mathbf{q}_s \parallel y$ axis. Here and in the following figures, we set (TB model) $\mu = -2.8t$ and $\alpha = 0.6t$. (b), c) Corresponding TB dispersions along k_x .

field angle with respect to planar axes, the Rashba dispersions of Eq. (3) in the parabolic model can be written explicitly as

$$\varepsilon_{\mathbf{k}\lambda}(\mathbf{b}) = \frac{1}{2m}(k + \lambda k_0)^2 - \tilde{\mu} + \lambda s_\alpha b \sin(\theta_{\mathbf{k}} - \phi), \quad (6)$$

where we defined $s_\alpha = \text{sign}(\alpha)$. This leads to Rashba Fermi sheets with a radius given by

$$k_F^\lambda(\theta_{\mathbf{k}}, \phi) = k_F^\lambda - \frac{1}{2\mu} k_F \lambda s_\alpha b \sin(\theta_{\mathbf{k}} - \phi), \quad (7)$$

where we assumed the physical hierarchy of energy scales according to ($b < |\alpha| < \mu < 2D_c$). An example for the geometry of Rashba Fermi surface sheets is shown in Fig. 1. The effect of the field on the two Rashba sheets may be easily understood by considering the relative change compared to the zero-field value k_F^λ as a function of the angle $\theta_{\mathbf{k}}$. For momentum (anti)parallel to the field with $\theta_{\mathbf{k}} = \phi + \pi$, ϕ there is no change and $k_F^\lambda(\theta_{\mathbf{k}}, \phi) = k_F^\lambda$. For the perpendicular case with $\theta_{\mathbf{k}} = \phi + \pi/2$, $\phi + 3\pi/2$, we have $k_F^\lambda(\theta_{\mathbf{k}}, \phi) = k_F^\lambda \mp \frac{1}{2} k_F \lambda s_\alpha (b/\mu)$. Thus the two Rashba sheets are shifted *perpendicular* to the field in opposite directions by the amount

$$q_s = \frac{b}{2\mu} k_F = \frac{m\mu_B B}{k_F} = \frac{b}{v_F}. \quad (8)$$

While the splitting of Rashba sheets is a measure for the coupling $|\alpha|$ their shifting perpendicular to \mathbf{B} is determined by field strength alone. These basic Rashba characteristics are shown in Fig. 1(a) as it results from the split and shifted dispersions in Figs. 1(b) and 1(c).

B. Superconducting state with finite momentum pairing

In this paper we do not discuss the possible mechanisms behind the superconducting gap formation in noncentrosymmetric compounds without inversion symmetry; for an excellent review see Ref. [29]. In these materials with Rashba spin-orbit coupling, phonons [30] as well as spin fluctuations [31–33] may be the driving mechanism for Cooper pair formation. In any case it is important to realize that, independent of the mechanism, the gap function contains spin-singlet as well as triplet components due to the inversion symmetry breaking presented by the Rashba term [29,34].

In addition here we consider the possibility of a common overall momentum $2\mathbf{q}$ of Cooper pairs due to the pair-breaking effect of the external field in conjunction with Rashba spin-orbit coupling. One should expect that the size of \mathbf{q} is correlated with the shift of the Rashba FS sheets [22] perpendicular to the field as given by Eq. (8). The real value of \mathbf{q} should be evaluated by the minimization of the condensation energy in the helical SC phase as is demonstrated in Sec. III. As mentioned in the introduction one may consider more general pair states with multiple pair momenta \mathbf{q}_i as possible ground states [23,25], in particular the LO-type “stripe phase” [21] with $(\mathbf{q}, -\mathbf{q})$ pair momenta. It was shown in Ref. [22] that the single \mathbf{q} helical phase can be stable in a large part of parameter space. We restrict to this case here as the most tractable representative case that shows the paired/depaird momentum space segmentation even though it may not be the true ground state for all parameter space. This has also a technical reason. For states with multiple \mathbf{q}_i pair vectors the explicit calculation of the QPI spectral function Eq. (51) becomes difficult to carry out. Furthermore the technique employed here is not able to treat cases like the stripe phase where the gap amplitude is modulated in real space.

Of the many possible choices of gap functions we use the minimal model introduced by Kaur *et al.* [21] which reduces to the spin-singlet form in the limit $\alpha = 0$. In the helical basis it is characterized by two gap functions $\Delta_{\mathbf{q}\lambda}^{\mathbf{k}}$ for the two Rashba sheets. The resulting mean field pair Hamiltonian in helicity representation is described by

$$H_{\text{MF}} = \sum_{\mathbf{k}\lambda} \varepsilon_{\mathbf{k}+\mathbf{q}\lambda} c_{\mathbf{k}+\mathbf{q}\lambda}^\dagger c_{\mathbf{k}+\mathbf{q}\lambda} - \frac{1}{2} \sum_{\mathbf{k}\lambda} [\Delta_{\mathbf{q}\lambda}^{\mathbf{k}} c_{\mathbf{k}+\mathbf{q}\lambda}^\dagger c_{-\mathbf{k}+\mathbf{q}\lambda}^\dagger + \Delta_{\mathbf{q}\lambda}^{\mathbf{k}*} c_{-\mathbf{k}+\mathbf{q}\lambda} c_{\mathbf{k}+\mathbf{q}\lambda}] \quad (9)$$

where the gap equation for the fully symmetric state of the helical phase as defined below is given by

$$\Delta_{\mathbf{q}\lambda}^{\mathbf{k}} = - \sum_{\mathbf{k}'\lambda'} V_{\lambda\lambda'}(\mathbf{k}\mathbf{k}') \langle c_{-\mathbf{k}'+\mathbf{q}\lambda'} c_{\mathbf{k}'+\mathbf{q}\lambda'} \rangle. \quad (10)$$

The summation has to be constrained over the segments of momentum space \mathbf{k}' where the pair states exist, i.e., where the quasiparticle excitations from the ground state have *positive* energy $E_{\mathbf{k}'\mathbf{q}\lambda}^r > 0$ [see Eq. (19)]. Due to this constraint which is indicated by the prime on the sum Eq. (10) is not practical for obtaining $\Delta_{\mathbf{q}\lambda}^{\mathbf{k}}(b)$. We rather pursue a different route later on by deriving an expression for the condensation energy as a functional of the helical gap and determine the latter and the pair vector by direct minimization of this functional.

Here we use the special simple gap model proposed by Kaur *et al.* [21] to which we restrict and we only briefly describe its ingredients. It assumes a singlet gap for the limiting case $\alpha = 0$ belonging to an irreducible representation Γ with a basis function $f_\Gamma(\mathbf{k})$. Turning on a finite α creates an additional \mathbf{k} dependence resulting from the helical spin structure. For small fields $b < |\alpha|$ the latter may be eliminated by a phase transformation $\Delta_{\mathbf{q}\pm}^{\Gamma\mathbf{k}} \rightarrow \pm \exp(\mp i\theta_{\mathbf{k}}) \Delta_{\mathbf{q}\pm}^{\Gamma\mathbf{k}}$ (we later keep the same symbol for the transformed gap) which is associated with a correspondingly transformed effective interaction that

takes the form [21]

$$\hat{V} = -\frac{V_\Gamma(\mathbf{k}\mathbf{k}')}{2}(\sigma_0 - \sigma_x) = -\frac{V_\Gamma(\mathbf{k}\mathbf{k}')}{2} \begin{bmatrix} 1 & -1 \\ -1 & 1 \end{bmatrix}, \quad (11)$$

where $V_\Gamma(\mathbf{k}\mathbf{k}') = V_0^\Gamma f_\Gamma(\mathbf{k})f_\Gamma(\mathbf{k}')$ ($V_0^\Gamma > 0$). Inserting this two-band pairing interaction into the gap equation [Eq. (10)] leads to the condition $\Delta_{\mathbf{q}^-}^{\Gamma\mathbf{k}} = -\Delta_{\mathbf{q}^+}^{\Gamma\mathbf{k}}$. The opposite sign of the two gaps is enforced by the opposite spin texture on the two Rashba bands. We want to investigate the appearance of unpaired low-energy normal quasiparticles in the helical phase and their signature in the QPI spectrum. As a first step we use a gap function representation that does not already by itself have nodal points or lines in order to avoid having both quasiparticles from the nodal regions and the depaired regions. Therefore, as in Ref. [21] we restrict to the trivial representation with $f_\Gamma(\mathbf{k}) = 1$ leading to (suppressing now Γ) a gap $\Delta_{\mathbf{q}\lambda}^{\Gamma\mathbf{k}} = \Delta_{\mathbf{q}\lambda}$ without explicit \mathbf{k} dependence. Then the total BCS Hamiltonian including the mean field energy constant is given by

$$H_{\text{BCS}} = H_{\text{MF}} + \frac{1}{2} \sum_{\mathbf{k}\lambda} \frac{|\Delta_{\mathbf{q}\lambda}|^2}{V_0}. \quad (12)$$

Introducing the Nambu spinors $\psi_{\mathbf{k}\mathbf{q}\lambda}^\dagger = (c_{\mathbf{k}+\mathbf{q}\lambda}^\dagger, c_{-\mathbf{k}+\mathbf{q}\lambda})$ we may write $H_{\text{MF}} = \hat{H}_{\text{MF}} + E_0$ where

$$\hat{H}_{\text{MF}} = \frac{1}{2} \sum_{\mathbf{k}\lambda} \psi_{\mathbf{k}\mathbf{q}\lambda}^\dagger \hat{h}_{\mathbf{k}\mathbf{q}\lambda} \psi_{\mathbf{k}\mathbf{q}\lambda}, \quad E_0 = \frac{1}{2} \sum_{\mathbf{k}\lambda} \varepsilon_{\mathbf{k}+\mathbf{q}\lambda}. \quad (13)$$

The constant term E_0 may be simplified using Eq. (15) below. The summation over λ eliminates the second term leading to $E_0 = \frac{1}{2} \sum_{\mathbf{k}\lambda} \xi_{\mathbf{k}+\mathbf{q}}$. The Hamilton matrix in Nambu space is given by

$$\hat{h}_{\mathbf{k}\mathbf{q}\lambda} = \begin{bmatrix} \varepsilon_{\mathbf{k}+\mathbf{q}\lambda} & -\Delta_{\mathbf{q}\lambda} \\ -\Delta_{\mathbf{q}\lambda}^* & -\varepsilon_{-\mathbf{k}+\mathbf{q}\lambda} \end{bmatrix}. \quad (14)$$

Using the symmetries $\xi_{\mathbf{k}} = \xi_{-\mathbf{k}}$ and $\mathbf{g}_{\mathbf{k}} = -\mathbf{g}_{-\mathbf{k}}$ the diagonal elements are obtained as

$$\begin{aligned} \varepsilon_{\mathbf{k}+\mathbf{q}\lambda}(\mathbf{b}) &= \xi_{\mathbf{k}+\mathbf{q}} + \lambda|\alpha\mathbf{g}_{\mathbf{k}+\mathbf{q}} + \mathbf{b}| = \xi_{\mathbf{k}+\mathbf{q}} + \lambda\zeta_{\mathbf{k}\mathbf{q}}^+, \\ \varepsilon_{-\mathbf{k}+\mathbf{q}\lambda}(\mathbf{b}) &= \xi_{\mathbf{k}-\mathbf{q}} + \lambda|\alpha\mathbf{g}_{\mathbf{k}-\mathbf{q}} - \mathbf{b}| = \xi_{\mathbf{k}-\mathbf{q}} + \lambda\zeta_{\mathbf{k}\mathbf{q}}^-, \end{aligned} \quad (15)$$

where we defined the auxiliary Rashba functions $\zeta_{\mathbf{k}\mathbf{q}}^\pm = |\alpha\mathbf{g}_{\mathbf{k}\pm\mathbf{q}} \pm \mathbf{b}|$ where both signs on the right are taken simultaneously as $+$ or $-$. We also introduce symmetric (s) and antisymmetric (a) combinations explicitly given by

$$\begin{aligned} \varepsilon_{\mathbf{k}\mathbf{q}\lambda}^s &= \frac{1}{2}(\varepsilon_{\mathbf{k}+\mathbf{q}\lambda} + \varepsilon_{-\mathbf{k}+\mathbf{q}\lambda}) \\ &= \frac{1}{2}(\xi_{\mathbf{k}+\mathbf{q}} + \xi_{\mathbf{k}-\mathbf{q}}) + \lambda\frac{1}{2}(\zeta_{\mathbf{k}\mathbf{q}}^+ + \zeta_{\mathbf{k}\mathbf{q}}^-) \equiv \xi_{\mathbf{k}\mathbf{q}}^s + \lambda\zeta_{\mathbf{k}\mathbf{q}}^s, \\ \varepsilon_{\mathbf{k}\mathbf{q}\lambda}^a &= \frac{1}{2}(\varepsilon_{\mathbf{k}+\mathbf{q}\lambda} - \varepsilon_{-\mathbf{k}+\mathbf{q}\lambda}) \\ &= \frac{1}{2}(\xi_{\mathbf{k}+\mathbf{q}} - \xi_{\mathbf{k}-\mathbf{q}}) + \lambda\frac{1}{2}(\zeta_{\mathbf{k}\mathbf{q}}^+ - \zeta_{\mathbf{k}\mathbf{q}}^-) \equiv \xi_{\mathbf{k}\mathbf{q}}^a + \lambda\zeta_{\mathbf{k}\mathbf{q}}^a. \end{aligned} \quad (16)$$

They fulfill the even/odd symmetry relations $\varepsilon_{-\mathbf{k}\mathbf{q}\lambda}^s = \varepsilon_{\mathbf{k}\mathbf{q}\lambda}^s$ and $\varepsilon_{-\mathbf{k}\mathbf{q}\lambda}^a = -\varepsilon_{\mathbf{k}\mathbf{q}\lambda}^a$, respectively. Here we defined $\xi_{\mathbf{k}\mathbf{q}}^{s,a} = \frac{1}{2}(\xi_{\mathbf{k}+\mathbf{q}} \pm \xi_{\mathbf{k}-\mathbf{q}})$ and $\zeta_{\mathbf{k}\mathbf{q}}^{s,a} = \frac{1}{2}(\zeta_{\mathbf{k}\mathbf{q}}^+ \pm \zeta_{\mathbf{k}\mathbf{q}}^-)$. In the formal limit of no Rashba coupling ($\alpha = 0$) this simplifies to $\zeta_{\mathbf{k}\mathbf{q}}^s = |\mathbf{b}|$ and $\zeta_{\mathbf{k}\mathbf{q}}^a = 0$. In this case the two Rashba bands $\varepsilon_{\mathbf{k}\lambda}$ [Eq. (3)] become the Zeeman split bands with effective spin index λ .

Now we can split the diagonal matrix elements in the Hamiltonian into symmetric and antisymmetric parts and using the symmetry relations we arrive at

$$\hat{h}_{\mathbf{k}\mathbf{q}\lambda} = \varepsilon_{\mathbf{k}\mathbf{q}\lambda}^a \tau_0 + \begin{bmatrix} \varepsilon_{\mathbf{k}\mathbf{q}\lambda}^s & -\Delta_{\mathbf{q}\lambda} \\ -\Delta_{\mathbf{q}\lambda}^* & -\varepsilon_{\mathbf{k}\mathbf{q}\lambda}^s \end{bmatrix}. \quad (17)$$

We note that in the following we will also use the property $\sum_{\mathbf{k}\lambda} \varepsilon_{\mathbf{k}\mathbf{q}\lambda}^a = 0$ which is due to the antisymmetry of $\varepsilon_{\mathbf{k}\mathbf{q}\lambda}^a$. Hereby the summation over \mathbf{k} runs over the paired and unpaired regions as defined below.

III. BOGOLIUBOV TRANSFORMATION FOR PAIRED AND DEPAIRED STATES

The first part in the \mathbf{k} -symmetrized Hamiltonian in Eq. (17) is already diagonal. The second part can now be diagonalized by a Bogoliubov transformation to quasiparticle states created by $\alpha_{\mathbf{k}\lambda}$ and $\beta_{\mathbf{k}\lambda}$ with the corresponding Hamiltonian expressed as

$$\begin{aligned} H_{\text{MF}} &= \frac{1}{2} \sum_{\mathbf{k}\lambda} [|E_{\mathbf{k}\mathbf{q}\lambda}^+| \alpha_{\mathbf{k}}^\dagger \alpha_{\mathbf{k}} + |E_{\mathbf{k}\mathbf{q}\lambda}^-| \beta_{\mathbf{k}}^\dagger \beta_{\mathbf{k}}] \\ &+ \frac{1}{2} \sum_{\mathbf{k}\lambda} \left\{ \begin{array}{l} \varepsilon_{\mathbf{k}\mathbf{q}\lambda}^s - E_{\mathbf{k}\mathbf{q}\lambda}; \quad E_{\mathbf{k}\mathbf{q}\lambda}^\tau > 0 \\ \varepsilon_{\mathbf{k}\mathbf{q}\lambda}^s + \varepsilon_{\mathbf{k}\mathbf{q}\lambda}^a; \quad E_{\mathbf{k}\mathbf{q}\lambda}^+ < 0 \\ \varepsilon_{\mathbf{k}\mathbf{q}\lambda}^s - \varepsilon_{\mathbf{k}\mathbf{q}\lambda}^a; \quad E_{\mathbf{k}\mathbf{q}\lambda}^- < 0 \end{array} \right\}. \end{aligned} \quad (18)$$

Here the quasiparticle energies are given by ($\tau = \pm, \bar{\tau} = \mp$):

$$\begin{aligned} E_{\mathbf{k}\mathbf{q}\lambda}^\tau &= E_{\mathbf{k}\mathbf{q}\lambda} + \tau \varepsilon_{\mathbf{k}\mathbf{q}\lambda}^a = E_{-\mathbf{k}\mathbf{q}\lambda}^{\bar{\tau}}, \\ E_{\mathbf{k}\mathbf{q}\lambda} &= [\varepsilon_{\mathbf{k}\mathbf{q}\lambda}^s + \Delta_{\mathbf{q}\lambda}^2]^{\frac{1}{2}} = E_{-\mathbf{k}\mathbf{q}\lambda}. \end{aligned} \quad (19)$$

When for a given \mathbf{k} and λ : $E_{\mathbf{k}\mathbf{q}\lambda}^\tau > 0$ ($\tau = \pm$), one has a stable Cooper pair state with pair momentum $2\mathbf{q}$ for this wave vector \mathbf{k} and band λ . If, on the other hand, $E_{\mathbf{k}\mathbf{q}\lambda}^+ < 0$ or $E_{\mathbf{k}\mathbf{q}\lambda}^- < 0$ the pair state is broken and only unpaired quasiparticle states exist at the wave vectors $\mathbf{k} + \mathbf{q}$ and $-\mathbf{k} + \mathbf{q}$. Note the remarkable fact that although for these wave vectors $|E_{\mathbf{k}\mathbf{q}\lambda}^\pm|$ are normal quasiparticle excitations their energy nevertheless contains the gap size $\Delta_{\mathbf{q}\lambda}$ determined by the paired states. This is because in the coherent helical ground state the unpaired electrons and holes also experience the pairing molecular field sustained by the paired electrons, even though they do not contribute to it. The mean field energy constant [last term in Eq. (18)] in the two cases is different because of the additional condensation energy in the paired state.

Therefore the corresponding Bogoliubov transformations for the two cases are also different: For the paired states it is given by [27]

$$E_{\mathbf{k}\mathbf{q}\lambda}^\tau > 0 : \begin{bmatrix} c_{\mathbf{k}+\mathbf{q}\lambda} \\ c_{-\mathbf{k}+\mathbf{q}\lambda}^\dagger \end{bmatrix} = \begin{bmatrix} u_{\mathbf{k}\lambda}^* & v_{\mathbf{k}\lambda} \\ -v_{\mathbf{k}\lambda}^* & u_{\mathbf{k}\lambda} \end{bmatrix} \begin{bmatrix} \alpha_{\mathbf{k}\lambda} \\ \beta_{\mathbf{k}\lambda}^\dagger \end{bmatrix}, \quad (20)$$

whereas for the depaired states it may be written as [27]

$$\begin{aligned} E_{\mathbf{k}\mathbf{q}\lambda}^+ < 0 : \begin{bmatrix} c_{\mathbf{k}+\mathbf{q}\lambda} \\ c_{-\mathbf{k}+\mathbf{q}\lambda}^\dagger \end{bmatrix} &= \begin{bmatrix} u_{\mathbf{k}\lambda}^* & v_{\mathbf{k}\lambda} \\ -v_{\mathbf{k}\lambda}^* & u_{\mathbf{k}\lambda} \end{bmatrix} \begin{bmatrix} \alpha_{\mathbf{k}\lambda}^\dagger \\ \beta_{\mathbf{k}\lambda}^\dagger \end{bmatrix}, \\ E_{\mathbf{k}\mathbf{q}\lambda}^- < 0 : \begin{bmatrix} c_{\mathbf{k}+\mathbf{q}\lambda} \\ c_{-\mathbf{k}+\mathbf{q}\lambda}^\dagger \end{bmatrix} &= \begin{bmatrix} u_{\mathbf{k}\lambda}^* & v_{\mathbf{k}\lambda} \\ -v_{\mathbf{k}\lambda}^* & u_{\mathbf{k}\lambda} \end{bmatrix} \begin{bmatrix} \alpha_{\mathbf{k}\lambda} \\ \beta_{\mathbf{k}\lambda} \end{bmatrix}. \end{aligned} \quad (21)$$

Explicitly the transformation coefficients are given by

$$u_{\mathbf{k}\lambda}^2 = \frac{1}{2} \left(1 + \frac{\varepsilon_{\mathbf{k}\mathbf{q}\lambda}^s}{E_{\mathbf{k}\mathbf{q}\lambda}} \right), \quad v_{\mathbf{k}\lambda}^2 = \frac{1}{2} \left(1 - \frac{\varepsilon_{\mathbf{k}\mathbf{q}\lambda}^s}{E_{\mathbf{k}\mathbf{q}\lambda}} \right). \quad (22)$$

These coefficients fulfill the well-known relations

$$u_{\mathbf{k}\lambda}^2 - v_{\mathbf{k}\lambda}^2 = \frac{\varepsilon_{\mathbf{k}\mathbf{q}\lambda}^s}{E_{\mathbf{k}\mathbf{q}\lambda}}, \quad 2u_{\mathbf{k}\lambda}v_{\mathbf{k}\lambda} = \frac{\Delta_{\mathbf{q}\lambda}}{E_{\mathbf{k}\mathbf{q}\lambda}}. \quad (23)$$

Note the important fact that only the *symmetrized* Rashba band energies $\varepsilon_{\mathbf{k}\mathbf{q}\lambda}^s$ appear in the transformation coefficients $u_{\mathbf{k}\lambda}$ and $v_{\mathbf{k}\lambda}$. However, both momentum-symmetric $\varepsilon_{\mathbf{k}\mathbf{q}\lambda}^s$ and antisymmetric $\varepsilon_{\mathbf{k}\mathbf{q}\lambda}^a$ contribute to the superconducting quasiparticle energies $E_{\mathbf{k}\mathbf{q}\lambda}^\tau$ in Eq. (19). This result of the analysis could not have been anticipated *a priori*.

The total BCS Hamiltonian, including the constant energy in Eq. (12), is then obtained as

$$\begin{aligned} H_{\text{BCS}} &= H_{\text{MF}} + \frac{1}{2} \sum_{\mathbf{k}\lambda} \left(\frac{|\Delta_{\mathbf{q}\lambda}|^2}{V_0} \right. \\ &= \frac{1}{2} \sum_{\mathbf{k}\lambda} (|E_{\mathbf{k}\mathbf{q}\lambda}^+| \alpha_{\mathbf{k}}^\dagger \alpha_{\mathbf{k}} + |E_{\mathbf{k}\mathbf{q}\lambda}^-| \beta_{\mathbf{k}}^\dagger \beta_{\mathbf{k}}) \\ &\quad \left. + \frac{1}{2} \sum_{\mathbf{k}\lambda} \left\{ \begin{array}{l} \varepsilon_{\mathbf{k}\mathbf{q}\lambda}^s - E_{\mathbf{k}\mathbf{q}\lambda} + \frac{|\Delta_{\mathbf{q}\lambda}|^2}{V_0} \\ \varepsilon_{\mathbf{k}\mathbf{q}\lambda}^s + \varepsilon_{\mathbf{k}\mathbf{q}\lambda}^a + \frac{|\Delta_{\mathbf{q}\lambda}|^2}{V_0} \\ \varepsilon_{\mathbf{k}\mathbf{q}\lambda}^s - \varepsilon_{\mathbf{k}\mathbf{q}\lambda}^a + \frac{|\Delta_{\mathbf{q}\lambda}|^2}{V_0} \end{array} \right\}. \end{aligned} \quad (24)$$

Here the second term (H_{BCS}) is equal to the total ground state energy $E_G(\mathbf{q}, \Delta_{\mathbf{q}\pm})$ of the helical FF-type state. As in Eq. (18) the sum extends over the upper value for paired states with $E_{\mathbf{k}\mathbf{q}\lambda}^\pm > 0$ whereas the lower values correspond to a sum only over the unpaired states with $E_{\mathbf{k}\mathbf{q}\lambda}^+ < 0$ or $E_{\mathbf{k}\mathbf{q}\lambda}^- < 0$, respectively. These conditional sums are indicated by the prime. The helical SC ground state energy may be rewritten explicitly as (see also Appendix A)

$$\begin{aligned} E_G(\mathbf{q}, \Delta_{\mathbf{q}\pm}) &= \frac{1}{2} \sum_{\lambda} \left[N \left(\frac{|\Delta_{\mathbf{q}\lambda}|^2}{V_0} \right) \right. \\ &\quad - \sum_{\mathbf{k}} (E_{\mathbf{k}\mathbf{q}\lambda} - \varepsilon_{\mathbf{k}\mathbf{q}\lambda}^s) + \sum_{\mathbf{k}} [E_{\mathbf{k}\mathbf{q}\lambda}^+ \Theta(-E_{\mathbf{k}\mathbf{q}\lambda}^+) \\ &\quad \left. + E_{\mathbf{k}\mathbf{q}\lambda}^- \Theta(-E_{\mathbf{k}\mathbf{q}\lambda}^-)] \right]. \end{aligned} \quad (25)$$

This energy functional should be minimized with respect to \mathbf{q} and $\Delta_{\mathbf{q}\pm}$ for Rashba coupling α and field strength b . It contains the possibilities of the helical ($\mathbf{q} \neq 0, |\Delta_{\mathbf{q}\lambda}| > 0$), BCS ($\mathbf{q} = 0, |\Delta_{0\lambda}| > 0$), and unpolarized normal ($b = 0, \mathbf{q} = 0, \Delta_{\mathbf{q}\lambda} = 0$) states. For the latter the ground state energy is

$$\begin{aligned} E_G^0 &= \frac{1}{2} \sum_{\mathbf{k}\lambda} (\varepsilon_{\mathbf{k}\lambda}^0 - |\varepsilon_{\mathbf{k}\lambda}^0|) = \sum_{\mathbf{k}\lambda} f_{\mathbf{k}\lambda} \varepsilon_{\mathbf{k}\lambda}^0, \\ \varepsilon_{\mathbf{k}\lambda}^0 &= \varepsilon_{\mathbf{k}\mathbf{q}\lambda}^s(\mathbf{q} = 0, b = 0) = \xi_{\mathbf{k}} + \lambda |\alpha \mathbf{g}_{\mathbf{k}}|, \end{aligned} \quad (26)$$

where $f_{\mathbf{k}} = \Theta(-\varepsilon_{\mathbf{k}\lambda}^0)$ is the zero temperature Fermi function for the unpolarized Rashba split bands $\varepsilon_{\mathbf{k}\lambda}^0$ [cf. Eq. (4)]. The minimization problem is greatly simplified by the equal size of the gaps $|\Delta_{\mathbf{q}\pm}| = \Delta_{\mathbf{q}}$ in the model defined by Eq. (11). Although strictly this holds only for $\mathbf{q}=0$ we will also keep

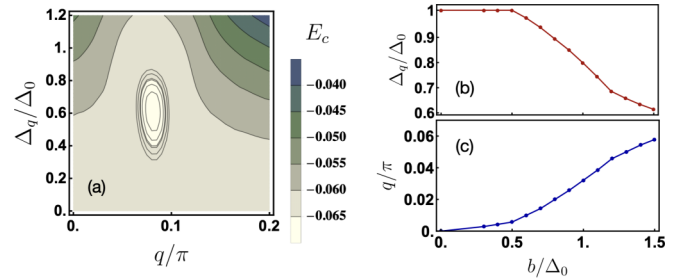


FIG. 2. (a) Contour plots of SC condensation energy $E_c < 0$ in the helical state in the (q, Δ_q) plane for typical field $\mathbf{b} = b\hat{\mathbf{x}}$ with $b < \alpha$. (b, c) Field dependence of helical gap size Δ_q , and (half-) pair momentum $\mathbf{q} = q\hat{\mathbf{y}}$, corresponding to the minimum in panel (a). Here and in the rest of the paper, we set $\Delta_0 = 0.3t$, $\alpha = 2\Delta_0 = 0.6t$.

this minimization constraint for the helical case. The pairing potential strength V_0 in Eq. (11) and in the ground state energy Eq. (25) is related to the BCS gap size Δ_0 and Rashba coupling α by the simplified single gap equation obtained from Eq. (10) in the limiting BCS case $b, q = 0$ at zero temperature. Then all momentum states are paired and the sum over \mathbf{k} is unrestricted:

$$\frac{1}{V_0} = \frac{1}{2N} \sum_{\mathbf{k}\lambda} \frac{1}{2E_{\mathbf{k}\lambda}} \Theta(\varepsilon_c - |\varepsilon_{\mathbf{k}\lambda}|), \quad (27)$$

where the BCS zero-field quasiparticle energy is $E_{\mathbf{k}\lambda} = [\varepsilon_{\mathbf{k}\lambda}^0 + \Delta_0^2]^{1/2}$. Here ξ_c is an effective cutoff of the pairing potential ($\Delta_0 < \xi_c < 2D_c$). In the following calculations the gap size Δ_0 is used directly as a fixed input parameter, then the cutoff may be absorbed in the effective coupling constant V_0 by deleting the Θ function. We stress again that Eq. (27) is only used for determination of V_0 (occurring below in E_c) as a function of input parameters Δ_0 and α .

For finding the ground state by numerical minimization it is useful to subtract the normal state energy from the ground state energy in Eq. (25) to obtain the superconducting condensation energy $E_c = E_G - E_G^0$ according to

$$\begin{aligned} E_c(\mathbf{q}, \Delta_{\mathbf{q}\pm}) &= \frac{1}{2} \sum_{\lambda} \left[N \left(\frac{|\Delta_{\mathbf{q}\lambda}|^2}{V_0} \right) - \sum_{\mathbf{k}} \{ (E_{\mathbf{k}\mathbf{q}\lambda} - |\varepsilon_{\mathbf{k}\lambda}^0|) \right. \\ &\quad + (\varepsilon_{\mathbf{k}\mathbf{q}\lambda}^s - \varepsilon_{\mathbf{k}\lambda}^0) + [E_{\mathbf{k}\mathbf{q}\lambda}^+ \Theta(-E_{\mathbf{k}\mathbf{q}\lambda}^+) \\ &\quad \left. + E_{\mathbf{k}\mathbf{q}\lambda}^- \Theta(-E_{\mathbf{k}\mathbf{q}\lambda}^-)] \right]. \end{aligned} \quad (28)$$

Note that the asymmetric $\varepsilon_{\mathbf{k}\mathbf{q}\lambda}^a$ Rashba energies of Eq. (16) enter only in the unpaired quasiparticle contribution (last term). Using the pure singlet gap constraint $\Delta_{\mathbf{q}\pm} = \pm \Delta_{\mathbf{q}}$ the minimization of $E_c(\mathbf{q}, \Delta_{\mathbf{q}})$ with respect to $\Delta_{\mathbf{q}}$ and \mathbf{q} for fixed field \mathbf{b} and Rashba coupling α determines the equilibrium gap $\Delta(\mathbf{q}, b, \alpha)$ and wave vector $\mathbf{q}(b, \alpha)$ characterizing the helical state. We have to keep in mind, however, that the pairing model of Eq. (11) is only strictly valid in the low field limit $b/\alpha \ll 1$. An example of the condensation energy minimum formation in the (q, Δ_q) plane and the resulting $\Delta_q(b), q(b)$ dependence for small fields and fixed α is shown in Fig. 2. The dependence of $\Delta_q(b)$ is directly correlated with

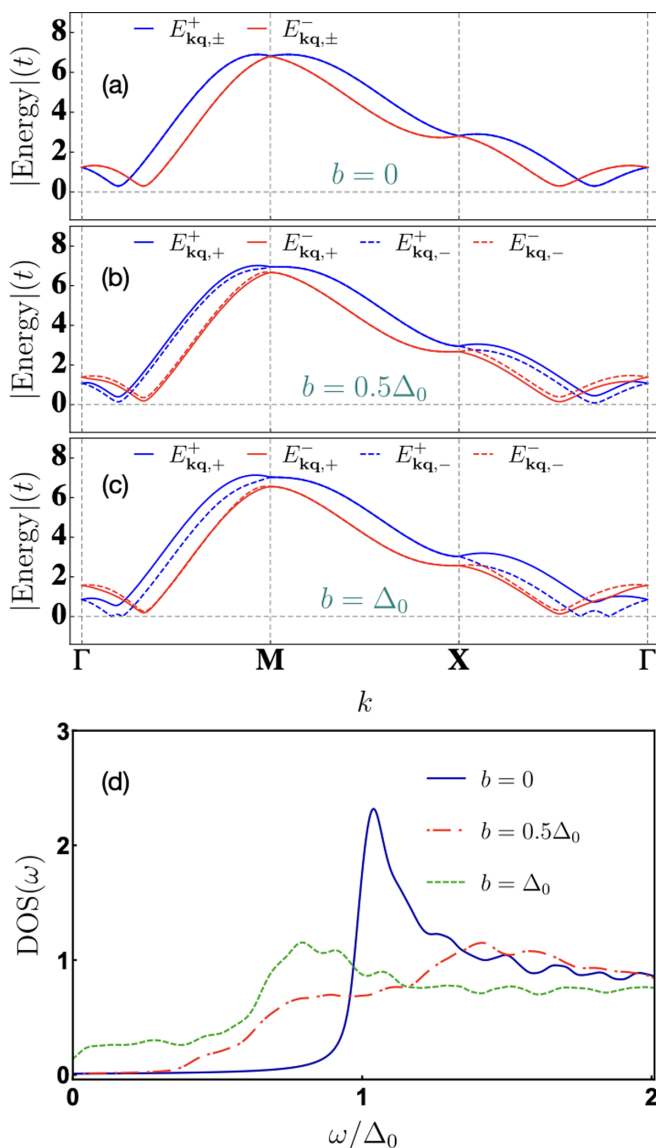


FIG. 3. (a–c) Quasiparticle dispersions $|E_{\mathbf{k}q\lambda}^\tau|$ in Eqs. (18) and (19) for different fields along the BZ path $\Gamma(0,0), M(\pi,\pi), X(0,\pi), \Gamma(0,0)$. (a) Fully paired BCS state with $E_{\mathbf{k}q\lambda}^\tau > 0$ for all \mathbf{k} . (b) One branch (dashed blue) touches zero leading to the appearance of unpaired states at the touch points. (c) Finite segment of unpaired states has formed due to $E_{\mathbf{k}q-}^+ < 0$ along ΓM and ΓX segments corresponding to the arc in the spectral function of Fig. 4. (d) Comparison of quasiparticle DOS, $\rho_{q\lambda}(\omega)$, corresponding to panels (a)–(c) for the Rashba-BCS state ($b=0, q=0, \Delta_0$) and helical state ($b, q \neq 0, \Delta_q$). The low energy DOS appears due to normal quasiparticles in the unpaired momentum space region characterized by the $|E_{\mathbf{k}q\lambda}^\tau| \simeq 0$ region in panels (a)–(c) and the arc regions in Fig. 4.

behavior of the excitation spectrum in Fig. 3. As long as low-energy quasiparticles from the depaired FS segments are absent $\Delta_q(b)$ stays constant, but it decreases rapidly when the quasiparticle dispersion touches zero energy for $b/\Delta_0 \simeq 0.5$ and the associated DOS becomes finite. Correspondingly the (half-)pair momentum $q(b)$ increases very slowly from BCS value $q(0) = 0$ in the low field regime and exhibits a crossover to rapid increase with b at $b/\Delta_0 \simeq 0.5$. This is similar to

the $q(b)$ behavior found in Refs. [24,35]. In Ref. [35] it was argued that above the crossover field $q(b) \sim q_s$ and below it is suppressed to $q(b) \sim (\alpha/|\mu|)q_s$ by a small prefactor. We also note that in Ref. [23] a vanishing $q(b)$ was obtained in the low field region.

IV. GREEN'S FUNCTIONS IN THE HELICAL RASHBA SUPERCONDUCTING STATE AND QUASIPARTICLE DOS

The Green's functions in the FF-type superconducting state are needed for the calculation of quasiparticle DOS and interference spectra. Using Eq. (17) we obtain

$$\begin{aligned} \hat{G}_{q\lambda}(\mathbf{k}, i\omega_n) &= (i\omega_n - \hat{h}_{\mathbf{k}q\lambda})^{-1} \\ &= \frac{1}{(i\omega_n - E_{\mathbf{k}q\lambda}^+)(i\omega_n + E_{\mathbf{k}q\lambda}^-)} \\ &\quad \times \begin{bmatrix} i\omega_n + \varepsilon_{\mathbf{k}q\lambda}^s - \varepsilon_{\mathbf{k}q\lambda}^a & -\Delta_{q\lambda} \\ -\Delta_{q\lambda}^* & i\omega_n - \varepsilon_{\mathbf{k}q\lambda}^s - \varepsilon_{\mathbf{k}q\lambda}^a \end{bmatrix}. \end{aligned} \quad (29)$$

The normal and anomalous Green's functions elements $G_{q\lambda}^{\tau,\tau'}(\mathbf{k}, i\omega_n)$ satisfy the following symmetry relations:

$$G_{q\lambda}^{11}(-\mathbf{k}, i\omega_n) = -G_{q\lambda}^{22}(\mathbf{k}, -i\omega_n), \quad (30)$$

and likewise

$$G_{q\lambda}^{12*}(-\mathbf{k}, i\omega_n) = G_{q\lambda}^{21}(\mathbf{k}, -i\omega_n). \quad (31)$$

The spectral function corresponding to the above Green's function is obtained as

$$\begin{aligned} A_{\mathbf{k}q}^\lambda(\omega) &= -\frac{1}{\pi} \text{Im}\{\text{tr}[\hat{G}_{q\lambda}(\mathbf{k}, \omega + i\eta)]\}_{\eta \rightarrow 0^+} \\ &= \sum_{\tau} \delta(\omega - E_{\mathbf{k}q\lambda}^\tau). \end{aligned} \quad (32)$$

Now using the symmetry relation $E_{-\mathbf{k}q\lambda}^\tau = E_{\mathbf{k}q\lambda}^{\bar{\tau}}$ (with $\tau = \pm$ and $\bar{\tau} = \mp$) one can define the symmetrized spectral function according to

$$\bar{A}_{\mathbf{k}q}^\lambda = \frac{1}{2}[A_{\mathbf{k}q}^\lambda(\omega) + A_{-\mathbf{k}q}^\lambda(\omega)] = \frac{1}{2}[A_{\mathbf{k}q}^\lambda(\omega) + A_{\mathbf{k}q}^\lambda(-\omega)]. \quad (33)$$

Using Eq. (32) they may be obtained for paired as well as unpaired regions as

$$\bar{A}_{\mathbf{k}q}^\lambda(\omega) = \frac{1}{2} \sum_{\tau} [\delta(\omega - |E_{\mathbf{k}q\lambda}^\tau|) + \delta(\omega + |E_{\mathbf{k}q\lambda}^\tau|)]. \quad (34)$$

This result agrees with the expression that may be directly inferred from the quasiparticle Hamiltonian of Eq. (18). Summation over quasiparticle momenta \mathbf{k} then leads to the quasiparticle DOS, $\rho_{q\lambda}(\omega)$, for Rashba band λ in the helical state with pair momentum $2\mathbf{q}$ according to

$$\rho_{q\lambda}(\omega > 0) = \frac{1}{2N} \sum_{\mathbf{k}} [\delta(\omega - |E_{\mathbf{k}q\lambda}^+|) + \delta(\omega - |E_{\mathbf{k}q\lambda}^-|)]. \quad (35)$$

This presentation for the DOS is perfectly adequate for its numerical evaluation and will in fact be used later. However, to elucidate the distinction between conduction bands without spin-orbit coupling ($\alpha = 0$) treated previously [20,27] and the

present Rashba split bands it is illuminating to evaluate this expression partly analytically, except for a remaining momentum angle integration. For that purpose we can simplify the expressions in Eq. (16) when $q/k_F \ll 1$ and $\mathbf{k} \simeq k_F \hat{\mathbf{k}}$ is close to the Fermi surface. Then $\xi_{\mathbf{k}}^s \simeq \xi_{\mathbf{k}}$ and $\xi_{\mathbf{k}}^a \simeq qv_F \cos(\theta_{\mathbf{k}} - \theta_{\mathbf{q}})$ with $v_F = k_F/m$ and the orthogonal pair momentum and field directions defined by $\theta_{\mathbf{q}} = \frac{\pi}{2}$ ($\mathbf{q} = q\hat{\mathbf{y}}$) and $\mathbf{b} = b\hat{\mathbf{x}}$. Furthermore this leads to $\mathbf{g}_{\mathbf{k}+\mathbf{q}} \simeq \mathbf{g}_{\mathbf{k}} \simeq (k_F^y, -k_F^x, 0)/k_F = (\sin \theta_{\mathbf{k}}, -\cos \theta_{\mathbf{k}}, 0)$. Using these approximations we get ($\xi_{\mathbf{k}} = \mathbf{k}^2/2m - \mu$)

$$\begin{aligned} \varepsilon_{\mathbf{kq}\lambda}^s &\equiv \varepsilon_{\mathbf{k}\lambda} = \xi_{\mathbf{k}} + \lambda|\alpha\mathbf{g}_{\mathbf{k}}| = \xi_{\mathbf{k}} + \lambda|\alpha|, \\ \varepsilon_{\mathbf{kq}\lambda}^a &= (v_F q + \lambda b) \sin \theta_{\mathbf{k}}. \end{aligned} \quad (36)$$

In this approximation the superconducting quasiparticle energies [Eq. (19)] then simplify to

$$E_{\mathbf{kq}\lambda}^{\tau} = [(\xi_{\mathbf{k}} + \lambda|\alpha|)^2 + \Delta_{\mathbf{q}\lambda}^2]^{\frac{1}{2}} + \tau(v_F q + \lambda b) \sin \theta_{\mathbf{k}}. \quad (37)$$

The quasiparticle DOS $\rho(\omega)$ may be evaluated [20,27] as

$$\begin{aligned} \rho_{\mathbf{q}}(\omega > 0) &= \frac{1}{4\pi} \sum_{\lambda} \rho_{\lambda}^n(0) \int_0^{2\pi} d\theta \int_0^{\hbar\omega_c} d\varepsilon \\ &\times \left[\delta(\omega - |E_{\mathbf{kq}\lambda}^+|) + \delta(\omega - |E_{\mathbf{kq}\lambda}^-|) \right], \end{aligned} \quad (38)$$

where $\rho_{\lambda}^n(0) = \rho_n(0) = m/2\pi$ is the normal state DOS equal for both Rashba bands. With the angle-independent bare Rashba dispersion $\varepsilon_{\mathbf{k}\lambda}^0 = \xi_{\mathbf{k}} + \lambda|\alpha|$ denoted by ε we can write

$$E_{\mathbf{kq}\lambda}^{\tau} = [\varepsilon^2 + \Delta_{\mathbf{q}\lambda}^2]^{\frac{1}{2}} + \tau(v_F q + \lambda b) \sin \theta_{\mathbf{k}}. \quad (39)$$

Introducing now $\hat{E}_{\theta q\lambda}^{\tau} = \omega - \tau(v_F q + \lambda b) \sin \theta$, the ε integration leads to the partial radial DOS at angle $\theta = \theta_{\mathbf{k}}$:

$$\hat{\rho}_{\mathbf{q}\lambda}(\omega, \theta) = \frac{1}{2} \left(\frac{|\hat{E}_{\theta q\lambda}^+|}{[|\hat{E}_{\theta q\lambda}^+|^2 - |\Delta_{\mathbf{q}\lambda}|^2]^{\frac{1}{2}}} + \frac{|\hat{E}_{\theta q\lambda}^-|}{[|\hat{E}_{\theta q\lambda}^-|^2 - |\Delta_{\mathbf{q}\lambda}|^2]^{\frac{1}{2}}} \right), \quad (40)$$

and the total DOS is then given by

$$\rho_{\mathbf{q}}(\omega) = \frac{1}{2\pi} \sum_{\lambda} \rho_{\lambda}^n(0) \int_0^{2\pi} d\theta \hat{\rho}_{\mathbf{q}\lambda}(\omega, \theta), \quad (41)$$

which has four contributions due to two quasiparticle branches for each of the two Rashba split bands characterized by $(\tau, \lambda) = (\pm, \pm)$. They have the same form and are determined by their different energies $\hat{E}_{\theta q\lambda}^{\tau}$ which are explicitly given by

$$\hat{E}_{\theta q\pm}^{\pm} = \omega \mp (v_F q + b) \sin \theta, \quad \hat{E}_{\theta q\pm}^{\mp} = \omega \mp (v_F q - b) \sin \theta. \quad (42)$$

Note that because of the helical spin polarization of Rashba states the Zeeman contribution for a fixed field direction is now also proportional to $\sin \theta$ since the spins are locked with respect to crystal axes for $|\alpha| \gg |\mathbf{b}|$. This is an essential difference to the inversion symmetric case without Rashba spin-orbit coupling where they can align parallel to the \mathbf{b} field [20,27] and therefore no dependence on the momentum angle θ appears in this case. An example of the quasiparticle DOS using the general form of Eq. (35) is shown in Fig. 3(d), together with the quasiparticle dispersions $|E_{\mathbf{kq}\lambda}^{\tau}|$ [Figs. 3(a)–3(c)] in Eq. (35). As the field increases and unpaired states appear in the helical phase the corresponding

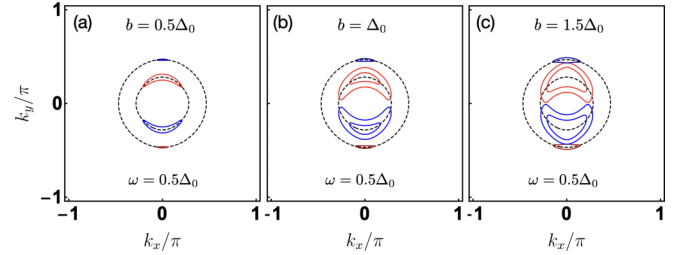


FIG. 4. Evolution of the spectral function in Eq. (34) with field b at frequency $\omega = 0.5\Delta_0$: (a) $b = 0.5\Delta_0$ with $q(b)/\pi = 0.005$, and $\Delta_q(b) = \Delta_0$; (b) $b = \Delta_0$ with $q(b)/\pi = 0.035$, and $\Delta_q(b) = 0.75\Delta_0$; (c) $b = 1.5\Delta_0$ with $q(b)/\pi = 0.06$, and $\Delta_q(b) = 0.59\Delta_0$. The dashed lines are corresponding to the bare (normal state) Rashba contours at $\omega = 0$ in zero field [Eq. (4)].

low-energy normal quasiparticles close to the zero energy line in Figs. 3(a)–3(c) gradually fill up the SC gap. It is important to note that a zero energy quasiparticle DOS appears although the helical SC order parameter has no nodes, either in \mathbf{k} space or in real space. This is rather a consequence of the presence of FS sheets of unpaired states defined by $|E_{\mathbf{kq}\lambda}^{\tau}| = \omega$. Their evolution with field b for constant frequency is shown in Fig. 4. The lenslike quasiparticle sheets appear close to the direction of the helical momentum \mathbf{q} and grow with field strength for both Rashba sheets $\lambda = \pm 1$.

V. QUASIPARTICLE INTERFERENCE SPECTRUM

Now we turn to the main object of this paper, the calculation of the quasiparticle interference spectrum in the helical phase which should show in a very straightforward manner the effect of the sofar hypothetical momentum-space segmentation of quasiparticles into paired and unpaired regions determined by field \mathbf{b} and Cooper pair momentum $2\mathbf{q}$. This effect contains the microscopic essence of the helical superconducting state. For this purpose it is also necessary to define a simple model for the surface-impurity scattering of quasiparticles and transform it to the basis of helical Rashba band states. In practice the impurities are adsorbed atoms or molecules at the surface with very small area concentration, and therefore the QPI spectrum is in fact determined by single-impurity site scattering processes [36]. These dilute surface impurities with weak scattering potential are not detrimental to the stability of the bulk FF-type helical state.

A. Normal and magnetic impurity scattering

We consider the two most frequent cases of normal charge (c) impurities and magnetic moment (m) impurities being responsible for electron scattering at the surface of the Rashba FF-type superconductor. In the normal state, using spin representation of conduction electrons the isotropic scattering from impurities located at random sites \mathbf{R}_i is described by

$$\begin{aligned} U_c(\mathbf{r} - \mathbf{R}_i) &= U_0 \sigma_0 \delta(\mathbf{r} - \mathbf{R}_i), \\ U_m(\mathbf{r} - \mathbf{R}_i) &= U_1 \sigma_z \delta(\mathbf{r} - \mathbf{R}_i) \end{aligned} \quad (43)$$

for the charge and exchange scattering, respectively. In the latter case we assumed an Ising-type classical local moment $\langle S_z(i) \rangle$ at site i oriented along the z direction by a uniaxial

potential, i.e., $U_1 = \frac{1}{2}J_{\text{ex}}\langle S_z(i) \rangle$, where J_{ex} is the on-site exchange constant. This leads to a Hamiltonian

$$H_{\text{imp}} = \sum_{i\mathbf{k}\mathbf{k}'\sigma} U_{\sigma} a_{\mathbf{k}'\sigma}^{\dagger} a_{\mathbf{k}\sigma} e^{i(\mathbf{k}'-\mathbf{k})\mathbf{R}_i}, \quad U_{\sigma} = U_0 + \sigma U_1 \quad (44)$$

in spin representation describing the scattering by random impurities at the surface where $\tilde{\mathbf{q}} = \mathbf{k}' - \mathbf{k}$ is the momentum transfer. It has to be transformed to the helical eigenstates of the Rashba bands defined by Eq. (5). Furthermore in the superconducting state we must use appropriate scattering matrices in Nambu (particle-hole) space according to the replacement $(U_0, U_1) \rightarrow (U_0\tau_z, U_1\tau_0)$ where τ_z and τ_0 are corresponding Pauli and unit matrices, respectively [37]. Then we obtain

$$H_{\text{imp}} = \sum_{i\mathbf{k}\mathbf{k}'\lambda\lambda'} \left[U_0 \tilde{V}_{\lambda\lambda'}^0(\mathbf{k}\mathbf{k}') \tau_z + U_1 \tilde{V}_{\lambda\lambda'}^1(\mathbf{k}\mathbf{k}') \tau_0 \right] c_{\mathbf{k}'\lambda}^{\dagger} c_{\mathbf{k}\lambda'} e^{i(\mathbf{k}'-\mathbf{k})\mathbf{R}_i}. \quad (45)$$

Here the momentum dependent scattering form factors $\tilde{V}_{\lambda\lambda'}^{0,1}(\mathbf{k}\mathbf{k}')$ are introduced by the transformation to helical eigenstates $|\mathbf{k}\lambda\rangle$ of each Rashba band according to Eq. (5). They are obtained from the transformation matrix in this equation according to

$$\begin{aligned} \tilde{V}_{\lambda\lambda'}^0(\mathbf{k}\mathbf{k}') &= \sum_{\sigma} S_{\sigma\lambda}^*(\mathbf{k}') S_{\sigma\lambda'}(\mathbf{k}), \\ \tilde{V}_{\lambda\lambda'}^1(\mathbf{k}\mathbf{k}') &= \sum_{\sigma} \sigma S_{\sigma\lambda}^*(\mathbf{k}') S_{\sigma\lambda'}(\mathbf{k}). \end{aligned} \quad (46)$$

Explicitly we obtain in helicity space $(\lambda\lambda')$ effective momentum-dependent c and m scattering potentials given, respectively, by

$$\begin{aligned} \{\tilde{V}_{\lambda\lambda'}^0(\mathbf{k}\mathbf{k}')\} &= \frac{1}{2} \begin{bmatrix} 1 + e^{i(\theta_{\mathbf{k}} - \theta_{\mathbf{k}'})} & i(e^{-i\theta_{\mathbf{k}}} - e^{-i\theta_{\mathbf{k}'}}) \\ i(e^{i\theta_{\mathbf{k}}} - e^{i\theta_{\mathbf{k}'}}) & 1 + e^{-i(\theta_{\mathbf{k}} - \theta_{\mathbf{k}'})} \end{bmatrix}, \\ \{\tilde{V}_{\lambda\lambda'}^1(\mathbf{k}\mathbf{k}')\} &= \frac{1}{2} \begin{bmatrix} 1 - e^{i(\theta_{\mathbf{k}} - \theta_{\mathbf{k}'})} & i(e^{-i\theta_{\mathbf{k}}} + e^{-i\theta_{\mathbf{k}'}}) \\ -i(e^{i\theta_{\mathbf{k}}} + e^{i\theta_{\mathbf{k}'}}) & -(1 - e^{-i(\theta_{\mathbf{k}} - \theta_{\mathbf{k}'})}) \end{bmatrix}. \end{aligned} \quad (47)$$

These scattering matrices are Hermitian, fulfilling the relations $\tilde{V}_{\lambda\lambda'}^{\kappa*}(\mathbf{k}, \mathbf{k}') = \tilde{V}_{\lambda'\lambda}^{\kappa}(\mathbf{k}', \mathbf{k})$ ($\kappa = 0, 1$). Since we use the periodic TB band model for the QPI calculation in the next section we also must use the periodic form of the phase angle $\theta_{\mathbf{k}} = \tan^{-1}(\sin k_y / \sin k_x)$ in the above expressions appropriate for the TB model. Note that one has to be careful to pick the right branches so that the polar angle covers

the whole interval $[0, 2\pi]$. This is guaranteed if we define $\theta_{\mathbf{k}}^0 = \tan^{-1}[\sin(k_y) / \sin(k_x)]$ and choose $\theta_{\mathbf{k}}$ in the whole BZ $-\pi \leq k_x, k_y \leq \pi$ in counterclockwise fashion in the four quadrants (I–IV) ($\pm k_x > 0, \pm k_y > 0$) according to

$$\begin{aligned} \text{(I)} \quad \theta_{\mathbf{k}} &= \theta_{\mathbf{k}}^0, & \text{(II)} \quad \theta_{\mathbf{k}} &= \pi - \theta_{\mathbf{k}}^0, \\ \text{(III)} \quad \theta_{\mathbf{k}} &= \theta_{\mathbf{k}}^0 + \pi, & \text{(IV)} \quad \theta_{\mathbf{k}} &= 2\pi - \theta_{\mathbf{k}}^0. \end{aligned} \quad (48)$$

In the helicity representation the scattering matrix includes nondiagonal interband terms $\lambda \neq \lambda'$ even though we started from a scattering potential diagonal in spin quantum numbers. Both momentum dependence and interband features of the scattering play a role in the QPI spectrum.

B. QPI spectrum in the Born approximation

The Fourier component of the surface charge modulation corresponding to momentum transfer $\tilde{\mathbf{q}} = \mathbf{k}' - \mathbf{k}$ (not to be confused with Cooper pair momentum $2\mathbf{q}$) and bias voltage $\omega = eV$ induced by the scattering from random impurities is given by (per impurity site) [26,37]

$$\begin{aligned} \delta N(\tilde{\mathbf{q}}, \omega) &= -\frac{1}{\pi} \text{Im}[\tilde{\Lambda}(\tilde{\mathbf{q}}, i\omega_n)]_{i\omega_n \rightarrow \omega + i\delta}, \\ \tilde{\Lambda}(\tilde{\mathbf{q}}, i\omega_n) &= \frac{1}{N} \sum_{\mathbf{k}\lambda\lambda'} [\tau_z \hat{G}_{\lambda}(\mathbf{k}, i\omega_n) \hat{t}_{\lambda\lambda'}(\mathbf{k}\mathbf{k}', i\omega_n) \hat{G}_{\lambda'}(\mathbf{k}', i\omega_n)]_{11}, \end{aligned} \quad (49)$$

where $\hat{t}_{\lambda\lambda'}(\mathbf{k}\mathbf{k}')(i\omega_n)$ is the scattering t matrix due to the impurity scattering potential [Eq. (45)] and the index (11) projects out the electron part of the Nambu matrix. Since the effective scattering in H_{imp} is momentum dependent due to helical transformation we treat it only in BA for weak scattering. As a matter of experience the QPI spectra in momentum space do not strongly depend on this simplification [37]. In the Born case the t matrix is frequency independent and simply given by

$$\hat{t}_{\lambda\lambda'}^c(\mathbf{k}\mathbf{k}') = U_0 \tilde{V}_{\lambda\lambda'}^0(\mathbf{k}\mathbf{k}') \tau_z, \quad \hat{t}_{\lambda\lambda'}^m(\mathbf{k}\mathbf{k}') = U_1 \tilde{V}_{\lambda\lambda'}^1(\mathbf{k}\mathbf{k}') \tau_0, \quad (50)$$

in the normal (charge) and exchange (magnetic) scattering (c and m) cases, respectively. Inserting this in Eq. (49), using the explicit FF-type Green's function [Eq. (29)], and defining $\tilde{\Lambda}_{(0,1)}(\tilde{\mathbf{q}}, i\omega_n) = U_{(0,1)} \Lambda_{0,1}(\tilde{\mathbf{q}}, i\omega_n)$ we obtain the final result of the QPI spectrum function (suppressing the pair momentum index \mathbf{q} everywhere)

$$\tilde{\Lambda}_{\kappa}(\tilde{\mathbf{q}}, i\omega_n) = \frac{1}{N} \sum_{\mathbf{k}\lambda\lambda'} \tilde{V}_{(1)\lambda\lambda'}^{\kappa}(\mathbf{k}\mathbf{k}') \left[\frac{(i\omega_n + \varepsilon_{\mathbf{k}\lambda}^s - \varepsilon_{\mathbf{k}\lambda}^a)(i\omega_n + \varepsilon_{\mathbf{k}'\lambda'}^s - \varepsilon_{\mathbf{k}'\lambda'}^a) - (-1)^{\kappa} \Delta_{\lambda} \Delta_{\lambda'}}{(i\omega_n - E_{\mathbf{k}\lambda}^+) (i\omega_n + E_{\mathbf{k}\lambda}^-) (i\omega_n - E_{\mathbf{k}'\lambda'}^+) (i\omega_n + E_{\mathbf{k}'\lambda'}^-)} \right] \quad (51)$$

for the two cases of normal ($c, \kappa = 0$) and magnetic ($m, \kappa = 1$) scattering, respectively, whereby the sign constraint $\Delta_+ = -\Delta_- = \Delta(q, b)$ for the gap functions has to be kept. In this sum we are using the BA scattering matrix from Eq. (47), the quasiparticle energies from Eq. (19), and the (anti)symmetrized normal state dispersions from Eq. (16). The value of the SC gap is obtained from the minimization

procedure of Eq. (28). Note that only the real part of the scattering matrix $\tilde{V}_{(1)\lambda\lambda'}^{\kappa}(\mathbf{k}\mathbf{k}') = \text{Re} \tilde{V}_{\lambda\lambda'}^{\kappa}(\mathbf{k}\mathbf{k}')$ which, due to the Hermiticity of Eq. (47), is symmetric under exchange of all indices enters the expression for $\tilde{\Lambda}_{\kappa}(\tilde{\mathbf{q}}, i\omega_n)$. Likewise the imaginary part $\tilde{V}_{(2)\lambda\lambda'}^{\kappa}(\mathbf{k}\mathbf{k}') = \text{Im} \tilde{V}_{\lambda\lambda'}^{\kappa}(\mathbf{k}\mathbf{k}')$ must be antisymmetric under this exchange and because the expression in parentheses in Eq. (51) is symmetric the summation over it

gives zero. The real symmetric scattering matrix elements in Eq. (51) in the charge ($\kappa = 0$) and magnetic ($\kappa = 1$) impurity cases are obtained from Eq. (47) as

$$\begin{aligned} \{\tilde{V}_{(1)\lambda\lambda'}^0(\mathbf{k}\mathbf{k}')\} &= \frac{1}{2} \begin{bmatrix} 1 + \cos(\theta_{\mathbf{k}} - \theta_{\mathbf{k}'}) & \sin \theta_{\mathbf{k}} - \sin \theta_{\mathbf{k}'} \\ -\sin \theta_{\mathbf{k}} + \sin \theta_{\mathbf{k}'} & 1 + \cos(\theta_{\mathbf{k}} - \theta_{\mathbf{k}'}) \end{bmatrix}, \\ \{\tilde{V}_{(1)\lambda\lambda'}^1(\mathbf{k}\mathbf{k}')\} &= \frac{1}{2} \begin{bmatrix} 1 - \cos(\theta_{\mathbf{k}} - \theta_{\mathbf{k}'}) & \sin \theta_{\mathbf{k}} + \sin \theta_{\mathbf{k}'} \\ \sin \theta_{\mathbf{k}} + \sin \theta_{\mathbf{k}'} & -1 + \cos(\theta_{\mathbf{k}} - \theta_{\mathbf{k}'}) \end{bmatrix}. \end{aligned} \quad (52)$$

The difference between the two is due to the different influence of helical spin texture in the two scattering mechanisms.

VI. DISCUSSION OF NUMERICAL QPI RESULTS: THE STM IMAGE OF MOMENTUM SPACE SEGMENTATION

The QPI method is well suited to observe the typical changes of quasiparticle sheets in momentum space connected with the appearance of the FF-type helical phase. The most characteristic feature is the reappearance of Fermi surface sheets for small frequencies $\omega < \Delta_0$ due to the pair breaking of combined Zeeman shift and Rashba splitting effects. The latter happens primarily for Cooper pairs with momenta $-\mathbf{k} + \mathbf{q}$, $\mathbf{k} + \mathbf{q}$ close to the direction of the shift vector \mathbf{q}_s of Rashba Fermi surfaces which is perpendicular to the applied field. As a function of applied QPI voltage $\omega = eV$ and field strength the unpaired sheets represented by the quasiparticle spectral functions undergo typical changes which contain information about the microscopic structure of the helical state. In particular it will give direct evidence for the Cooper pair momentum $2\mathbf{q}$ being perpendicular to the applied field and more importantly under favorable conditions it should be possible to estimate its magnitude from analyzing characteristic momenta $\tilde{\mathbf{q}}_i$ of the QPI image.

In the following we will therefore discuss the typical QPI charge images $\delta N(\tilde{\mathbf{q}}, \omega)$ expected in experiment which we derived in the previous section for the charge and magnetic impurity scattering cases. It will turn out that the two are to a certain extent complementary. They will present mainly the same features due to the same quasiparticle energy denominators in Eq. (51) but with different intraband/interband intensity distribution due to the coherence factors in the numerator which contain different signs $(-1)^\kappa$ for the two scattering mechanisms. Furthermore the momentum dependence of effective scattering matrices in Eq. (52) is different in the two cases. In order to achieve sufficient numerical accuracy for detailed QPI image structure we have to use an enhanced size for the SC gap scale Δ_0 which will be set to 0.5α throughout.

First, as a reference, we will briefly discuss the QPI image in the zero-field BCS case with conventional Cooper pairs, i.e., $\mathbf{q} = 0$, of Fig. 5 (see also Ref. [20]). In Fig. 5(a) the spectral function presents two almost isotropic and featureless Rashba split Bogoliubov quasiparticle sheets (full lines) which show an additional splitting due to the doubling of particle-hole branches by the superconducting gap. For frequencies ω slightly above the gap size their radii are close to the Fermi wave vectors k_F^λ of the normal state (dashed lines) given in Sec. II A. In this case it is well known that the QPI image generated by all scattering events across the two

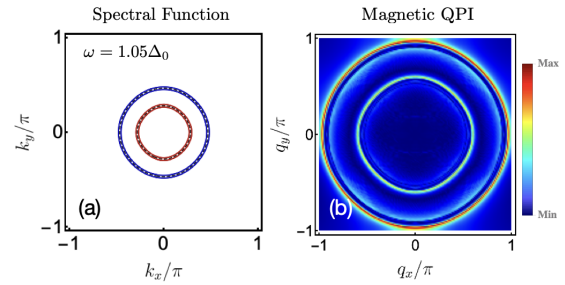


FIG. 5. Reference spectral function (a) and QPI spectrum (b) for the Rashba-BCS phase ($b, q = 0$; $\Delta_0 = 0.3t$; $\alpha = 2\Delta_0$) for $\omega \simeq \Delta_0$.

spheres is again spherical with the doubling of the radius to approximately $2k_F^\lambda$ as is indeed seen in Fig. 5. For frequencies ω slightly below the gap Δ_0 this QPI image is rapidly extinguished.

In distinction in the helical phase with superconducting order parameter $\Delta_{\mathbf{q}\lambda}$ corresponding to finite pair momentum $2\mathbf{q}$ the regions in \mathbf{k} space where Bogoliubov energy $E_{\mathbf{k}\mathbf{q}\lambda}^+ < 0$ or $E_{\mathbf{k}\mathbf{q}\lambda}^- < 0$ are depaired and have normal quasiparticle energies $|E_{\mathbf{k}\mathbf{q}\lambda}^+|$ or $|E_{\mathbf{k}\mathbf{q}\lambda}^-|$ starting from zero and hence lead to quasiparticle sheets even for $\omega < |\Delta_{\mathbf{q}\lambda}|$. They are presented by plotting the spectral functions of Eq. (34) for various bias voltage $eV = \omega$ or frequencies in the left columns of Figs. 6 and 7 (see also Fig. 4). The segmentation of \mathbf{k} space into paired regions without low-energy quasiparticles (small $|k_y|$) and unpaired regions with quasiparticle sheets (large $|k_y|$) is clearly seen for the different frequencies. Here the inner/outer Rashba

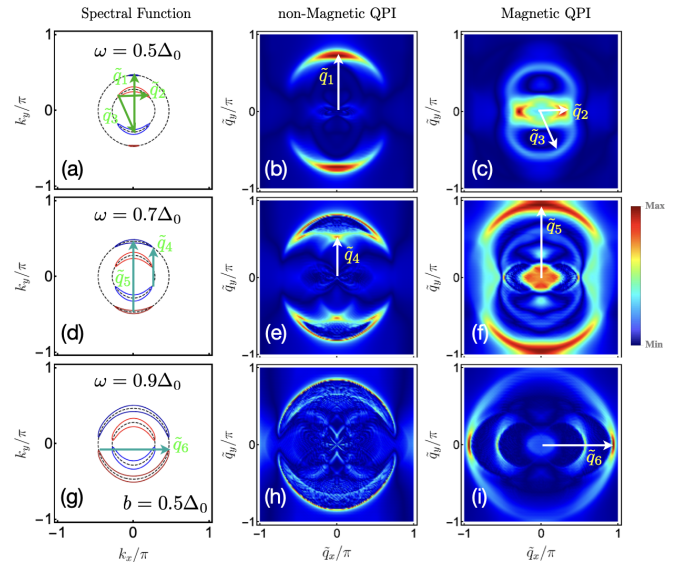


FIG. 6. Evolution of the spectral function (a, d, g) and corresponding QPI spectrum for the Rashba-helical FF-type phase: (b, e, h) charge scattering QPI and (c, f, i) magnetic scattering QPI, with frequency [first row, $\omega = 0.5\Delta_0$; second row, $\omega = 0.7\Delta_0$; third row, $\omega = 0.9\Delta_0$], and at field $b = 0.5\Delta_0$ with $q(b)/\pi = 0.005$, and $\Delta_q(b) = \Delta_0$. Note that interband scatterings are contributed mostly from the nonmagnetic impurities, whereas magnetic impurities mainly lead to intraband scatterings.

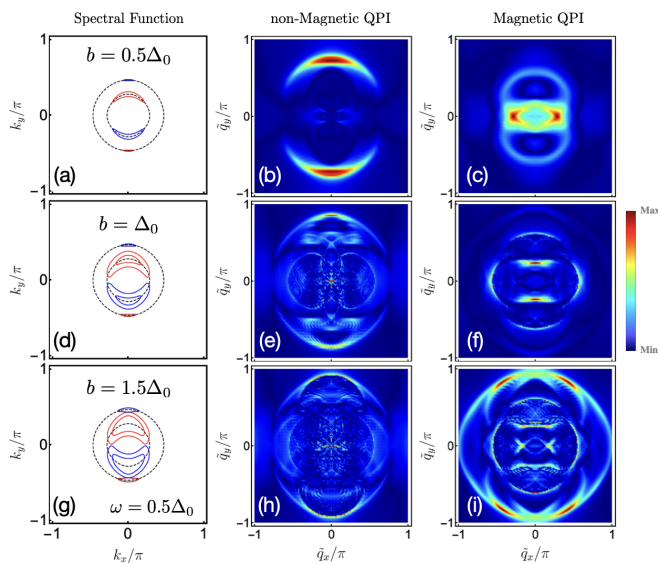


FIG. 7. Evolution of the spectral function (a, d, g) and corresponding QPI spectra for the Rashba-helical FF-type phase: (b, e, h) charge scattering QPI and (c, f, i) magnetic scattering QPI, with field b and at frequency $\omega = 0.5\Delta_0$. The first, second, and third rows correspond to $b = 0.5\Delta_0$ with $q(b)/\pi = 0.005$, and $\Delta_q(b) = \Delta_0$; $b = \Delta_0$ with $q(b)/\pi = 0.035$, and $\Delta_q(b) = 0.75\Delta_0$; and $b = 1.5\Delta_0$ with $q(b)/\pi = 0.06$, and $\Delta_q(b) = 0.59\Delta_0$, respectively.

FSs (dashed lines) correspond to $\lambda = \pm 1$ and the blue/red bent lenses to quasiparticle sheets $|E_{\mathbf{kq}\lambda}^\tau| = \omega$ correspond to $\tau = \pm 1$. For small ω [panel (a)] the first sheet appears in the inner Rashba band $\lambda = -1$ and then on the outer one $\lambda = +1$ increasing in size with increasing ω [panels (d) and (g)]. They end at the tip positions characterized by polar angles $\theta_{\mathbf{k}}$ where $E_{\mathbf{kq}\lambda}^\tau = \omega$. The large curvature at these points leads to a small group velocity and hence large DOS contribution from their vicinity. Hence they may appear prominently in the integrated QPI spectrum, however as mentioned before the momentum dependent scattering matrix elements also influence the intensity.

From a comparison of the model calculation for the segmented Fermi surfaces (more precisely equal-energy surfaces at bias voltage $\omega = eV$) and its associated theoretical QPI spectrum with the experimental one it is possible to investigate the details of the pair-breaking effect in the helical phase on the quasiparticle spectrum. In Fig. 6 we give a comparison between calculated spectral functions (left column) in the helical phase and its associated predicted QPI spectra and show their evolution as a function of frequency or bias voltage for constant field (center and right column for charge and magnetic impurity scattering, respectively). We can identify a selection of the characteristic possible intraband ($\lambda = \lambda'$) and interband ($\lambda \neq \lambda'$) scattering vectors $\tilde{\mathbf{q}}_i$ ($i = 1-6$) defined in the left column as intense or at least enhanced features in the QPI image in the center and right column. These correspondences are indicated in the panels with white arrows. Particularly prominent and easy to identify are the tip-to-tip scattering vectors $\tilde{\mathbf{q}}_4$ for nonmagnetic and $\tilde{\mathbf{q}}_2$ and $\tilde{\mathbf{q}}_6$ for magnetic scattering. The other characteristic QPI vectors map out the whole Fermi surface arc segments of the spectral function

in the left column. In reverse this means that an experimental QPI spectrum in the helical phase of a Rashba superconductor allows one to reconstruct the segmented Fermi surface sheets that appear as a consequence of the depairing of Cooper pairs the momenta of which are primarily oriented along the helical \mathbf{q} vector. It is also noteworthy that the intensity distribution of the QPI spectrum is to a certain extent complementary for nonmagnetic and magnetic scattering, emphasizing different regions of $\tilde{\mathbf{q}}$ space: The interband scatterings appear most prominent for nonmagnetic impurities, whereas magnetic impurities mainly lead to intraband scatterings. This is due to the different coherence factors (numerators) in Eq. (51) and angular dependences of the effective scattering matrices in Eq. (52) for the two cases.

Figure 7 presents results for the field evolution of QPI as an alternative to the previous one. Now the frequency is fixed to $\omega = 0.5\Delta_0$ and the field is varied in the low field regime $b < \alpha$ of the helical phase (the zero-field BCS case is already presented in Fig. 5 and the first row is identical to the one in Fig. 7). Whereas in the previous figure the quasiparticle sheets simply extend their dimension along the Rashba circle with increasing ω now the increasing field changes their shape and may lead to a doubling. This means the field evolution of the QPI spectrum in central and right columns are also distinct. It is again possible to identify characteristic scattering vectors in the latter that correspond to those connecting the various sheets in the spectral function.

Altogether our analysis demonstrates that an experimental magnetic/nonmagnetic QPI spectrum and its frequency and field evolution should contain enough information to map out the segmented quasiparticle sheets in the helical phase with finite Cooper pair momentum which is at the heart of this FF-type Rashba superconducting state.

Finally one may ask whether the information contained in the QPI images allows one to extract the size of the Cooper pair momentum \mathbf{q} as a function of field from the experimental data. We note that none of the thermodynamic experimental methods can achieve this. Since the \mathbf{q} vector for moderate fields has only a small fraction of the BZ extension and because it enters in a complicated manner in the spectrum of Eq. (51) one may not expect a direct identification in the QPI images of Figs. 6 and 7. However, it is possible to derive an empirical relation for its estimation from experimental quantities for small fields. For this purpose we note that the frequency dependent tips of the spectral functions at polar angles $\theta_{\mathbf{k}\lambda}^\tau$ in the left column of Figs. 6 and 7 are characterized by the following conditions: (i) their quasiparticle energy fulfils $E_{\mathbf{kq}\lambda}^\tau = \omega$ and (ii) they lie very close to the original (dashed lines) Rashba Fermi spheres with radius k_F^λ (Sec. II A). On these spheres Eq. (37) reduces to

$$E_{\mathbf{kq}\lambda}^\tau \simeq \Delta_{\mathbf{q}} + \tau(v_F q + \lambda b) \sin \theta_{\mathbf{k}\lambda}^\tau \equiv \omega. \quad (53)$$

We can determine the angles $\theta_{\mathbf{k}\lambda}^\tau$ at the tip positions from the geometry depicted in Figs. 6(a), 6(d) and 6(g). To be specific let us consider the upper part ($\tau = -1$) of the inner sheet ($\lambda = -1$) extended along the Rashba sphere with radius k_F^- . Its right (θ_R) and left ($\theta_L = \pi - \theta_R$) tips are connected by characteristic vector $\tilde{\mathbf{q}}_2$ which is prominently seen in the corresponding magnetic QPI spectrum [Fig. 6(c)]. Then we

obtain $\cos \theta_R = \frac{\tilde{q}_2}{2k_F}$. The sheet with a value $0 < \theta_R < \pi/2$ exists only when $\omega > \Delta_q - (v_F q - b) \equiv \omega_0$ or equivalently when $\omega' = \omega - \omega_0 > 0$. Then we may resolve Eq. (53) to obtain a phenomenological

$$q(b, \omega') = \frac{b}{v_F} + \frac{\omega'}{1 - \sin \theta_R(\omega')}, \quad (54)$$

where the first term is the Rashba FS shift q_s of Eq. (8). The Cooper pair momentum $q(b)$ is then obtained from the extrapolation to small $\omega' \rightarrow 0$ where $\sin \theta_R(\omega') = [1 - \frac{\tilde{q}_2^2}{2k_F^2}]^{\frac{1}{2}} \rightarrow 1$ in this limit. It has to be obtained from the experimentally observed $\tilde{q}_2(\omega')$. A similar procedure may be applied to other characteristic QPI vectors $\tilde{\mathbf{q}}_i$ to obtain $q(b)$. In principle this opens a way to determine the Cooper pair momentum $2q(b)$ directly from STM-QPI experiments.

VII. CONCLUSION AND OUTLOOK

In this paper we investigated microscopic features of the helical phase in Rashba superconductors with isotropic and equal magnitude of the gap function on the two Rashba bands. The latter have helical spin texture enforced by the strong Rashba spin-orbit coupling. In a magnetic field they are shifted perpendicular to the field by an amount proportional to its size. Therefore Cooper pairing in a state with nonvanishing pair momentum $2\mathbf{q}$ will be favored.

Using the approximations for large Rashba coupling we derived the condensation energy as a function of \mathbf{q} . Minimization leads to the dependence of pair momentum and gap size on the applied field. At the same time we computed the quasiparticle energies in the helical state. Their most interesting aspect is a segmentation of momentum space into regions where Cooper pairs are stable and gapped Bogoliubov excitations exist and other regions spread around the direction of the overall pair momentum where pair breaking due to large kinetic energy destroys the Cooper pairs and leads to normal low-energy quasiparticles with corresponding Fermi surface sheets. These are present despite the fact that the gap $\Delta_{\mathbf{q}\lambda}^{\mathbf{k}} = \Delta_{\mathbf{q}\lambda}$ is nodeless in \mathbf{k} space and real space.

We investigate this basic microscopic structure of the helical state, a coherent superposition of paired and unpaired states with associated peculiar evolution of Fermi surface (surfaces of constant energy) topology as a function of field and frequency. In this paper we have shown that the technique of quasiparticle interference is well suited to address this central property of Rashba superconductors with finite momentum Cooper pairing. It is able to monitor the appearance of the segmented Fermi surface sheets of unpaired quasiparticles as a function of field strength and bias voltage until they evolve into those of the normal state Rashba sheets for large values of these tuning parameters. Due to the helical frozen spin texture the QPI images obtained for charge and magnetic impurity scattering on the surface show considerable difference and are complementary in the intensity distribution. Furthermore following some of the characteristic wave vectors of the segments one may derive an estimate for the size of the pair momentum $2\mathbf{q}$ which is not accessible by other experimental means.

The FF-type helical phase in the Rashba superconductor is more amenable to such QPI investigations because it appears already for small fields and does not require the extremely large fields of the genuine FF phase in the inversion symmetric superconductors. It may also occur more frequently since there is a considerable number of inversion symmetry breaking (noncentrosymmetric) superconductors known by now. In particular such QPI investigations for the helical phase should be possible in layered superconductors with strong 2D character which has been assumed in our analysis.

ACKNOWLEDGMENT

A.A. acknowledges the support of the Max Planck POSTECH/Hsinchu Center for Complex Phase Materials.

APPENDIX A: DERIVATION OF THE SUPERCONDUCTING CONDENSATION ENERGY

Here we give a brief derivation of Eq. (28) used to find the $(\mathbf{q}, \Delta_{\mathbf{q}})$ values by minimization. First we note that the ground state energy $\langle H_{\text{BCS}} \rangle$ for the paired states [first row in curly brackets in Eq. (24)] may also be written in different equivalent forms given below:

$$\begin{aligned} \langle H_{\text{BCS}} \rangle_{\text{paired}} &= \frac{1}{2} \sum'_{\mathbf{k}\lambda} \left[\varepsilon_{\mathbf{k}\mathbf{q}\lambda}^s - E_{\mathbf{k}\mathbf{q}\lambda} + \frac{|\Delta_{\mathbf{q}\lambda}|^2}{V_0} \right] \\ &= \frac{1}{2} \sum'_{\mathbf{k}\lambda} \left[2\varepsilon_{\mathbf{k}\mathbf{q}\lambda}^s v_{\mathbf{k}\lambda}^2 - \frac{|\Delta_{\mathbf{q}\lambda}|^2}{V_0} \right] \\ &= \frac{1}{2} \sum'_{\mathbf{k}\lambda} \left[\varepsilon_{\mathbf{k}\mathbf{q}\lambda}^s - E_{\mathbf{k}\mathbf{q}\lambda} + \frac{|\Delta_{\mathbf{q}\lambda}|^2}{2E_{\mathbf{k}\mathbf{q}\lambda}} \right] \\ &= \frac{1}{2} \sum'_{\mathbf{k}\lambda} \left[\varepsilon_{\mathbf{k}\mathbf{q}\lambda}^s - \frac{\varepsilon_{\mathbf{k}\mathbf{q}\lambda}^2}{E_{\mathbf{k}\mathbf{q}\lambda}} - \frac{|\Delta_{\mathbf{q}\lambda}|^2}{2E_{\mathbf{k}\mathbf{q}\lambda}} \right]. \quad (\text{A1}) \end{aligned}$$

Here the prime denotes summation over paired states only with $E_{\mathbf{k}\mathbf{q}\lambda}^{\pm} > 0$. Using the first form above the total ground state energy obtained from the mean field approximation and Bogoliubov transformation is originally given by

$$\begin{aligned} E_G(\mathbf{q}, \Delta_{\mathbf{q}\pm}) &= \frac{1}{2} \sum_{\lambda} \left[N \left(\frac{|\Delta_{\mathbf{q}\lambda}|^2}{V_0} \right) + \sum_{\mathbf{k}} \varepsilon_{\mathbf{k}\mathbf{q}\lambda}^s \right. \\ &\quad \left. + 2 \sum_{\mathbf{k}} \varepsilon_{\mathbf{k}\mathbf{q}\lambda}^a \Theta(-E_{\mathbf{k}\mathbf{q}\lambda}^+) \right. \\ &\quad \left. - \sum_{\mathbf{k}} E_{\mathbf{k}\mathbf{q}\lambda}^- \Theta(E_{\mathbf{k}\mathbf{q}\lambda}^+) \Theta(E_{\mathbf{k}\mathbf{q}\lambda}^-) \right]. \quad (\text{A2}) \end{aligned}$$

In the zero-field normal state ($b = 0$, $\mathbf{q} = 0$, $\Delta_{\mathbf{q}\lambda} = 0$) where $\varepsilon_{\mathbf{k}\mathbf{q}\lambda}^a = 0$ and $E_{\mathbf{k}\mathbf{q}\lambda}^{\pm} = |\varepsilon_{\mathbf{k}\lambda}^0| > 0$ this ground state energy reduces to

$$\begin{aligned} E_G^0 &= \frac{1}{2} \sum_{\mathbf{k}\lambda} (\varepsilon_{\mathbf{k}\lambda}^0 - |\varepsilon_{\mathbf{k}\lambda}^0|) = \sum_{\mathbf{k}\lambda} f_{\mathbf{k}\lambda} \varepsilon_{\mathbf{k}\lambda}^0, \\ \varepsilon_{\mathbf{k}\lambda}^0 &= \varepsilon_{\mathbf{k}\mathbf{q}\lambda}^s(\mathbf{q} = 0, b = 0) = \xi_{\mathbf{k}} + \lambda |\alpha \mathbf{g}_{\mathbf{k}}|, \quad (\text{A3}) \end{aligned}$$

where $f_{\mathbf{k}} = \Theta(-\varepsilon_{\mathbf{k}\lambda}^0)$ is the zero temperature Fermi function for the unpolarized Rashba split bands $\varepsilon_{\mathbf{k}\lambda}^0$ [cf. Eq. (4)]. The

condensation energy for the minimization is then given by $E_c = E_G - E_G^0$.

To obtain a more symmetric form for E_G and E_c we now use the identity

$$\Theta(E_{\mathbf{k}q\lambda}^+) \Theta(E_{\mathbf{k}q\lambda}^-) = 1 - \Theta(-E_{\mathbf{k}q\lambda}^+) - \Theta(-E_{\mathbf{k}q\lambda}^-), \quad (\text{A4})$$

which holds because both $E_{\mathbf{k}q\lambda}^{\pm}$ cannot be simultaneously negative since their sum $E_{\mathbf{k}q\lambda}^+ + E_{\mathbf{k}q\lambda}^- = E_{\mathbf{k}q\lambda} > 0$. Inserting this into Eq. (A2) and using $\sum_{\mathbf{k}} \varepsilon_{\mathbf{k}q\lambda}^a = 0$ we obtain after some simple rearrangements the symmetrized form of the ground state energy

$$E_G(\mathbf{q}, \Delta_{\mathbf{q}\pm}) = \frac{1}{2} \sum_{\lambda} \left[N \left(\frac{|\Delta_{\mathbf{q}\lambda}|^2}{V_0} \right) - \sum_{\mathbf{k}} (E_{\mathbf{k}q\lambda} - \varepsilon_{\mathbf{k}q\lambda}^s) + \sum_{\mathbf{k}} [E_{\mathbf{k}q\lambda}^+ \Theta(-E_{\mathbf{k}q\lambda}^+) + E_{\mathbf{k}q\lambda}^- \Theta(-E_{\mathbf{k}q\lambda}^-)] \right] \quad (\text{A5})$$

given before in Eq. (25). Subtracting the normal state energy of Eq. (A3) we obtain again the condensation energy expression given in Eq. (28).

APPENDIX B: PROOF OF VANISHING CHARGE CURRENT

In the normal state of an interacting electron system the total charge current must be zero according to a generalized Bloch theorem [38]. In the BCS superconductor with only $(\mathbf{k}, -\mathbf{k})$ pairs present this is still true. It is known that even in the FF state without Rashba coupling the total charge current vanishes although the pairs have finite common momentum $2\mathbf{q}$. This is due to the fact that the current is the pair-momentum derivative of the total energy which must vanish in the ground state [27]. Here we show that this still holds for the case of finite Rashba coupling. The charge current operator is commonly given in terms of Bloch operators creating spin σ_z eigenstates [27]. After a unitary transformation to helical states ($\lambda = \pm$) in the Rashba system we obtain (in units of e)

$$\mathbf{J}_{\mathbf{q}}^c = \frac{1}{m} \sum_{\mathbf{k}} [(\mathbf{k} + \mathbf{q}) c_{\mathbf{k}+\mathbf{q}+}^{\dagger} c_{\mathbf{k}+\mathbf{q}+} - (\mathbf{k} - \mathbf{q}) c_{-\mathbf{k}+\mathbf{q}-}^{\dagger} c_{-\mathbf{k}+\mathbf{q}-}]. \quad (\text{B1})$$

Transforming to Bogoliubov quasiparticle states with Eqs. (20) and (21) we obtain for the y component ($q_y = q, k_y = k$) of the current

$$\langle J_q^c \rangle = \frac{1}{2m} \sum_{\mathbf{k}\lambda} [2q |v_{\mathbf{k}\lambda}|^2 \theta_H(E_{\mathbf{k}q\lambda}^+) \theta_H(E_{\mathbf{k}q\lambda}^-) + (q+k) \theta_H(-E_{\mathbf{k}q\lambda}^+) + (q-k) \theta_H(-E_{\mathbf{k}q\lambda}^-)]. \quad (\text{B2})$$

Now we consider again the total ground state energy Eq. (24), using an equivalent form for the paired term according to Eq. (A1) and the relation $\sum_{\mathbf{k}\lambda} \varepsilon_{\mathbf{k}q\lambda}^a = 0$:

$$\langle H_{\text{BCS}} \rangle = \frac{1}{2} \sum_{\mathbf{k}\lambda} \left\{ \begin{array}{l} 2\varepsilon_{\mathbf{k}q\lambda}^s v_{\mathbf{k}\lambda}^2 - \frac{|\Delta_{\mathbf{q}\lambda}|^2}{V_0}, \quad E_{\mathbf{k}q\lambda}^{\tau} > 0 \\ \varepsilon_{\mathbf{k}+\mathbf{q}\lambda}(b) + \frac{|\Delta_{\mathbf{q}\lambda}|^2}{V_0}, \quad E_{\mathbf{k}q\lambda}^+ < 0 \\ \varepsilon_{\mathbf{k}-\mathbf{q}\lambda}(-b) + \frac{|\Delta_{\mathbf{q}\lambda}|^2}{V_0}, \quad E_{\mathbf{k}q\lambda}^- < 0 \end{array} \right\}. \quad (\text{B3})$$

Then, using similar small- q approximation as in Sec. IV, we arrive at the identity

$$\frac{\partial \langle H_{\text{BCS}} \rangle}{\partial q} = \frac{1}{2} \sum_{\mathbf{k}\lambda} \left\{ \begin{array}{l} 2q v_{\mathbf{k}\lambda}^2, \quad E_{\mathbf{k}q\lambda}^{\tau} > 0 \\ q+k, \quad E_{\mathbf{k}q\lambda}^+ < 0 \\ q-k, \quad E_{\mathbf{k}q\lambda}^- < 0 \end{array} \right\} = \langle J_q^c \rangle. \quad (\text{B4})$$

Because the condensation energy of Eq. (28) is given by $E_c(q, \Delta_q) = E_G(q, \Delta_q) - E_G^0$ where $E_G = \langle H_{\text{BCS}} \rangle$ is the helical ground state energy [Eq. (25)] and E_G^0 is the constant normal state energy [Eq. (26)] it means that $\langle J_q^c \rangle = \partial E_c(q, \Delta_q) / \partial q$, i.e., the charge current in the helical state with (q, Δ_q) is equal to the q derivative of the condensation energy in that state. Since the true values of (q, Δ_q) are those where $E_c(q, \Delta_q)$ is a minimum [Fig. 2(a)] it means that $\partial E_c(q, \Delta_q) / \partial q = 0$ vanishes and therefore the charge current $\langle J_q^c \rangle$ [Eq. (B2)] in the helical state with the true (q, Δ_q) also vanishes, similar to the inversion symmetric case [27]. We conclude that also in the presence of the Rashba coupling we have vanishing charge current $\langle J_q^c \rangle = 0$ in the ground state. This situation may be different for the spin current which is already nonzero in the zero-field phase of the Rashba superconductor [39].

[1] P. Fulde and R. A. Ferrell, Superconductivity in a strong spin-exchange field, *Phys. Rev.* **135**, A550 (1964).
 [2] A. I. Larkin and Y. N. Ovchinnikov, Nonuniform state of superconductors, *Zh. Eksp. Teor. Fiz.* **47**, 1136 (1964) [*Sov. Phys. JETP* **20**, 762 (1965)].
 [3] H. Shimahara, Fulde-Ferrell state in quasi-two-dimensional superconductors, *Phys. Rev. B* **50**, 12760 (1994).
 [4] H. Shimahara, Structure of the Fulde-Ferrell-Larkin-Ovchinnikov state in two-dimensional superconductors, *J. Phys. Soc. Jpn.* **67**, 736 (1998).
 [5] D. E. Sheehy and L. Radzihovsky, BEC-BCS crossover, phase transitions and phase separation in polarized resonantly-paired superfluids, *Ann. Phys. (NY)* **322**, 1790 (2007).

[6] D. E. Sheehy, Fulde-Ferrell-Larkin-Ovchinnikov state of two-dimensional imbalanced Fermi gases, *Phys. Rev. A* **92**, 053631 (2015).
 [7] S. Takada, Superconductivity in a molecular field. II: Stability of Fulde-Ferrel phase, *Prog. Theor. Phys.* **43**, 27 (1970).
 [8] Y. Matsuda and H. Shimahara, Fulde-Ferrell-Larkin-Ovchinnikov state in heavy fermion superconductors, *J. Phys. Soc. Jpn.* **76**, 051005 (2007).
 [9] Q. Wang, C.-R. Hu, and C.-S. Ting, Impurity-induced configuration-transition in the Fulde-Ferrell-Larkin-Ovchinnikov state of a d -wave superconductor, *Phys. Rev. B* **75**, 184515 (2007).

- [10] L. W. Gruenberg and L. Gunther, Fulde-Ferrell Effect in Type-II Superconductors, *Phys. Rev. Lett.* **16**, 996 (1966).
- [11] H. Adachi and R. Ikeda, Effects of Pauli paramagnetism on the superconducting vortex phase diagram in strong fields, *Phys. Rev. B* **68**, 184510 (2003).
- [12] R. Lortz, Y. Wang, A. Demuer, P. H. M. Böttger, B. Bergk, G. Zwicknagl, Y. Nakazawa, and J. Wosnitzer, Calorimetric Evidence for a Fulde-Ferrell-Larkin-Ovchinnikov Superconducting State in the Layered Organic Superconductor $\kappa - (\text{BEDT} - \text{TTF})_2\text{Cu}(\text{NCS})_2$, *Phys. Rev. Lett.* **99**, 187002 (2007).
- [13] H. Mayaffre, S. Krämer, M. Horvatić, C. Berthier, K. Miyagawa, K. Kanoda, and V. F. Mitrović, Evidence of Andreev bound states as a hallmark of the FFLO phase in $\kappa - (\text{BEDT} - \text{TTF})_2\text{Cu}(\text{NCS})_2$, *Nat. Phys.* **10**, 928 (2014).
- [14] P. Burger, F. Hardy, D. Aoki, A. E. Böhmer, R. Eder, R. Heid, T. Wolf, P. Schweiss, R. Fromknecht, M. J. Jackson, C. Paulsen, and C. Meingast, Strong Pauli-limiting behavior of H_{c2} and uniaxial pressure dependencies in KFe_2As_2 , *Phys. Rev. B* **88**, 014517 (2013).
- [15] D. A. Zocco, K. Grube, F. Eilers, T. Wolf, and H. v. Löhneysen, Pauli-Limited Multiband Superconductivity in KFe_2As_2 , *Phys. Rev. Lett.* **111**, 057007 (2013).
- [16] A. Bianchi, R. Movshovich, C. Capan, P. G. Pagliuso, and J. L. Sarrao, Possible Fulde-Ferrell-Larkin-Ovchinnikov Superconducting State in CeCoIn_5 , *Phys. Rev. Lett.* **91**, 187004 (2003).
- [17] K. Kumagai, H. Shishido, T. Shibauchi, and Y. Matsuda, Evolution of Paramagnetic Quasiparticle Excitations Emerged in the High-Field Superconducting Phase of CeCoIn_5 , *Phys. Rev. Lett.* **106**, 137004 (2011).
- [18] R. Combescot, Introduction to FFLO phases and collective mode in the BEC-BCS crossover, in *Ultra-Cold Fermi Gases*, edited by M. Inguscio, W. Ketterle, and C. Salomon, Proceedings of the International School of Physics “Enrico Fermi” Vol. 164 (IOS, Amsterdam, 2007), p. 697.
- [19] G. Zwicknagl and J. Wosnitzer, *BCS: 50 Years* (World Scientific, Singapore, 2011), Chap. 14, p. 337.
- [20] A. Akbari and P. Thalmeier, Momentum space imaging of the FFLO state, *New J. Phys.* **18**, 063030 (2016).
- [21] R. P. Kaur, D. F. Agterberg, and M. Sigrist, Helical Vortex Phase in the Noncentrosymmetric CePt_3Si , *Phys. Rev. Lett.* **94**, 137002 (2005).
- [22] D. F. Agterberg and R. P. Kaur, Magnetic-field-induced helical and stripe phases in Rashba superconductors, *Phys. Rev. B* **75**, 064511 (2007).
- [23] F. Loder, A. P. Kampf, and T. Kopp, Superconductivity with Rashba spin-orbit coupling and magnetic field, *J. Phys.: Condens. Matter* **25**, 362201 (2013).
- [24] Y. Nakamura and Y. Yanase, Multi-orbital Fulde-Ferrell-Larkin-Ovchinnikov state in SrTiO_3 heterostructures, *J. Phys. Soc. Jpn.* **84**, 024714 (2015).
- [25] G. Zwicknagl, S. Jahns, and P. Fulde, Critical magnetic field of ultra-thin superconducting films and interfaces, *J. Phys. Soc. Jpn.* **86**, 083701 (2017).
- [26] A. Akbari and P. Thalmeier, Rashba spin-orbit coupling effects in quasiparticle interference of noncentrosymmetric superconductors, *Europhys. Lett.* **102**, 57008 (2013).
- [27] Q. Cui, C.-R. Hu, J. Y. T. Wei, and K. Yang, Conductance characteristics between a normal metal and a two-dimensional Fulde-Ferrell-Larkin-Ovchinnikov superconductor: The Fulde-Ferrell state, *Phys. Rev. B* **73**, 214514 (2006).
- [28] P. Thalmeier and A. Akbari, Gapped Dirac cones and spin texture in thin film topological insulator, *Phys. Rev. Research* **2**, 033002 (2020).
- [29] M. Sigrist, Introduction to unconventional superconductivity in noncentrosymmetric metals, *AIP Conf. Proc.* **1162**, 55 (2009).
- [30] B. Wiendlocha, R. Szczśniak, A. P. Durajski, and M. Muras, Pressure effects on the unconventional superconductivity of noncentrosymmetric LaNiC_2 , *Phys. Rev. B* **94**, 134517 (2016).
- [31] Y. Yanase and M. Sigrist, Superconductivity and magnetism in non-centrosymmetric system: Application to CePt_3Si , *J. Phys. Soc. Jpn.* **77**, 124711 (2008).
- [32] T. Takimoto and P. Thalmeier, Triplet Cooper pair formation by anomalous spin fluctuations in non-centrosymmetric superconductors, *J. Phys. Soc. Jpn.* **78**, 103703 (2009).
- [33] S. P. Mukherjee and T. Takimoto, Order parameter with line nodes and s_{\pm} -wave symmetry for the noncentrosymmetric superconductor $\text{Li}_2\text{Pt}_3\text{B}$, *Phys. Rev. B* **86**, 134526 (2012).
- [34] F. Loder, A. P. Kampf, T. Kopp, and D. Braak, Momentum-space spin texture in a topological superconductor, *Phys. Rev. B* **96**, 024508 (2017).
- [35] Y. Yanase and M. Sigrist, Magnetic properties in noncentrosymmetric superconductors with and without antiferromagnetic order, *J. Phys. Soc. Jpn.* **76**, 124709 (2007).
- [36] L. Capriotti, D. J. Scalapino, and R. D. Sedgewick, Wave vector power spectrum of the local tunneling density of states: Ripples in a d -wave sea, *Phys. Rev. B* **68**, 014508 (2003).
- [37] A. Akbari and P. Thalmeier, Full t-matrix approach to quasiparticle interference in non-centrosymmetric superconductors, *Eur. Phys. J. B* **86**, 495 (2013).
- [38] D. Bohm, Note on a theorem of Bloch concerning possible causes of superconductivity, *Phys. Rev.* **75**, 502 (1949).
- [39] A. B. Vorontsov, I. Vekhter, and M. Eschrig, Surface Bound States and Spin Currents in Noncentrosymmetric Superconductors, *Phys. Rev. Lett.* **101**, 127003 (2008).